BOOK CHAPTER:
To Appear in a book on "Dynamic Fracture Mechanics", (H.H Aliabadi, editor)(1995), Computational Mechanics Publications, Southampton, UK, Boston USA
ISBN 1 85312 3499 (Southampton)
ISBN 1 56252 2671 (BOSTON)

Chapter

Investigation of transient effects for dynamically initiating and growing cracks under stress wave loading conditions

Cheng Liu[a,b] **& Ares J. Rosakis**[a]

[a] *Graduate Aeronautical Laboratories, California Institute of Technology, Pasadena, CA 91125, USA*

[b] *Currently at Los Alamos National Laboratory, Los Alamos, NM 87545, USA*

Abstract

The problem of a semi-infinite crack, loaded by a planar stress wave, which after a finite delay time, extends with a constant speed, is revisited. We use this particular problem to investigate the question of dominance of the mode-I asymptotic elastodynamic crack-tip fields. The complete full field analytical solution of stresses surrounding the stationary and moving crack-tip is obtained using the procedure outlined by Freund (1973 and 1990). This analytical solution is compared to the asymptotic structure obtained by Freund and Rosakis (1992) and by Liu and Rosakis (1992), and the coefficients of the higher order transient asymptotic representation are thus determined. The normal traction ahead of the moving crack-tip is studied and compared to the field represented either by the square root singular term (K_I^d-dominant term) or by the higher order transient asymptotic expansion. The result shows that the higher order transient asymptotic expansion is necessary to describe the near-tip field at times close to the event of crack initiation, or at locations relatively far away from the crack-tip. This observation suggests that in the event

where transient effects are severe and cannot be neglected, the K_I^d-dominant field (square root singular field) should give way to the higher order transient asymptotic representation. The plate impact experimental configuration utilized by Ravichandran and Clifton (1989) and by Prakash and Clifton (1992) to study dynamic fracture, can be modeled mathematically by the solution given in Section 2. In Section 3, we provide an interpretation to their experimental observations. The result of our initial simulations which assume constant crack-tip speed, shows that the higher order transient representation successfully captures the overall features of the experimental results. Subsequently, we relax the restriction of constant crack-tip velocity. Motivated by the experimental measurements made by Zehnder and Rosakis (1990), a fracture criterion that relates the dynamic stress intensity factor to the speed of the propagating crack, is introduced. By solving the crack-tip equation of motion, all time-dependent quantities in the higher order transient asymptotic representation are determined. The final simulation of the plate impact experiments shows that the fully transient asymptotic field can describe the measured particle velocities very well. It is found that the experimental observations can be interpreted most accurately by including the effects of crack-tip acceleration and rapid changes of the dynamic stress intensity factor associated with the initial stages of crack growth.

1 Introduction

In the last decade, extensive theoretical and experimental studies have been carried out on the subject of dynamic fracture under stress wave loading conditions. Due to the high loading rates which exist during a dynamic fracture event, the effects of material inertia and strain rate sensitivity cannot be neglected, and as a result the material may exhibit totally different fracture behavior than the one exhibited under quasi-static loading regimes. Because of the complex transient nature of the crack initiation, growth and arrest problems, complete analytical solutions of even elastodynamic problems are very scarce. Moreover, these analytical solutions are only valid for those situations corresponding to very special geometrical configurations and loading conditions so that the mathematical models are tractable. Some of the theoretical and experimental studies on the subject are described below.

Baker (1962) studied the transient problem of a semi-infinite crack suddenly appearing in a pre-stretched elastic body and simultaneously propagating with a constant speed. He used the Laplace transform and

the Wiener-Hopf techniques to obtain the distribution of normal tractions ahead of the moving crack-tip, as well as the asymptotic leading term of the stress field surrounding the crack-tip. This leading term which is square root singular in stresses and whose amplitude is the dynamic stress intensity factor $K_I^d(t)$, will be referred to in this investigation as the "K_I^d-dominant field." Similarly, the region near the crack-tip where the stress field is well approximated by the square root singular term will be called "region of K_I^d-dominance." Achenbach and Nuismer (1971) observed that Baker's result was essentially the solution for the case of a planar step-stress wave with a wavefront parallel to the semi-infinite crack impinging on the initially stationary crack. When the stress wave hits the crack, the crack begins to grow with a constant speed. They then extended the solution to include incident waves of arbitrary stress profile, and also to include the case of oblique incidence. The unrealistic restriction of instant crack growth when the incident stress wave reaches the crack-tip in the above solutions was relaxed by Freund (1973), who introduced a finite delay time between the two events of stress wave arrival at the crack and the onset of crack extension. By using an elegant superposition procedure, Freund obtained the expression for the dynamic stress intensity factor at the running crack-tip, and also generalized this expression to the case of non-uniform crack growth speeds. He found that for an unbounded body subjected to time-independent loading, the dynamic stress intensity factor at the running crack-tip can be expressed as a *universal* function of instantaneous crack-tip speed multiplied by the equilibrium stress intensity factor for the given applied loading and the instantaneous amount of crack growth.

Since these early theoretical studies have revealed that the stress field near the tip of a propagating crack can be represented in terms of a dynamic stress intensity factor, analogous to that for a static crack, a large number of experimental investigations has attempted to measure this parameter for various specimen configurations and for various loading conditions. The eventual goal of these studies was to use the dynamic stress intensity factor concept in the formulation of a dynamic fracture criterion. From the experimental point of view, Ravi-Chandar and Knauss (1982) studied the dynamic fracture of a semi-infinite crack in an unbounded body subjected to a uniform step pressure applied on the crack faces. The solution of this problem can be obtained from the solution for the problem studied by Freund (1973) and described above. By using the optical method of caustics, and by interpreting the experimental results on the assumption of the existence of a K_I^d-dominant field within which

the caustic pattern is formed, they found that when the crack starts to propagate, a discrepancy exists between experimentally inferred dynamic stress intensity factors and the theoretical predictions. For the same problem studied by Ravi-Chandar and Knauss, Ma and Freund (1986) observed that for a point which is fixed with respect to the moving crack-tip, a surprisingly long time is needed for the stress intensity factor controlled field (K_I^d-dominant field) to be fully established. Their observation suggested that optical measurements (by caustics or otherwise) performed at finite distances from the crack-tip and at times close to crack initiation should not be interpreted on the basis of the assumption of the existence of a K_I^d-dominant field. The fact that the classical analysis of caustics assumes K_I^d-dominance whereas the deformation field does not conform with this assumption, provided an explanation in the discrepancy between the theoretical and the experimentally inferred stress intensity factors in the experiments by Ravi-Chandar and Knauss (1982). Further evidence for this phenomenon was provided by Krishnaswamy and Rosakis (1991), who used a bifocal caustics arrangement to directly investigate the accuracy of the classical analysis of caustics in measuring dynamic stress intensity factors in the presence of transients. Their results identified the short comings of the assumption of K_I^d-dominance and provided insight of the conditions under which this assumption fails in laboratory size specimens. With the suspicion of the lack of K_I^d-dominance, as further emphasized by Krishnaswamy and Rosakis (1991), the dependability of stress intensity factor histories measured from various experimental techniques is still questionable.

By relaxing the assumption of K_I^d-dominance, Freund and Rosakis (1992) and Rosakis *et al.* (1991) have recently obtained a higher order transient asymptotic expansion for the stress field surrounding the mode-I moving crack-tip. The leading term of this expansion corresponds to the classical square root singular stress field (K_I^d-dominant field). The higher order, less singular terms in this interpretation are found to involve coefficients that are functions of the time derivatives of crack-tip speed as well as the time derivatives of $K_I^d(t)$. When highly transient conditions exist, there exist regions near the crack-tip where the higher order terms may be as important as the leading square root singular contribution, and if so, K_I^d-dominance will be absent. Such cases are typically ones involving large crack-tip accelerations or sudden crack initiation or crack arrest events that may be a result of discrete stress wave arrivals. Based on these results, Liu *et al.* (1993) re-examined the optical method of caustics and provided a new interpretation technique for the

analysis of caustic patterns and the accurate inference of the dynamic stress intensity factors in the presence of transients, in cases where strict K_I^d-dominance is absent. The analysis of Freund and Rosakis (1992) was generalized for the case of a mixed-mode crack propagating along an arbitrarily curved path by Liu and Rosakis (1992). This analysis provided the higher order transient asymptotic representation of the elastodynamic field surrounding the crack-tip. The higher order terms were found to depend on the time derivatives of the complex dynamic stress intensity factor $K_I^d + iK_{II}^d$, the crack-tip acceleration, as well as on the local value of the crack path curvature. For generally anisotropic solids the same issues for a transiently propagating mode-I crack were addressed by Willis (1992).

The asymptotic analyses described above provide the spatial structure of the field near the crack-tip when transient conditions exist. As a result, they are necessary for the accurate interpretation of optical high speed photography measurements performed in laboratory specimens of finite size where steady state conditions are usually the exception rather than the rule. Such measurements may be performed by means of optical techniques such as photoelasticity, caustics or the Coherent Gradient Sensor (CGS). A discussion of the experimental verification of the existence and the influence of transient higher order terms in dynamic fracture is given by Krishnaswamy *et al.* (1992) and by Rosakis (1993).

The desire of producing very high loading rates and easily interpretable dynamic crack initiation and growth experiments has recently motivated Ravichandran and Clifton (1989) to devise a plate impact experimental configuration for the investigation of dynamic fracture. This configuration is capable of producing extremely high loading rates $\dot{K}_I^d \sim 10^8 \mathrm{MPa}\sqrt{\mathrm{m}}\cdot\mathrm{sec}^{-1}$ under stress wave loading and plane strain conditions. The specimen configuration and loading condition they used, simulates the problem of a plane strain semi-infinite crack subjected to a planar stress pulse of finite duration. Consequently the experimental observations can be directly compared with the analytical results given by Freund (1973). By monitoring the particle velocity at a point some distance away from the initial crack-tip, Prakash and Clifton (1992) have observed some interesting phenomena which cannot be explained merely by the existence of a pure K_I^d-dominant elastodynamic field.

The ultimate purpose of this study is to provide an interpretation to the observation made by Prakash and Clifton (1992) for a suddenly initiating and transiently propagating crack, within the framework of

linear elastic dynamic fracture mechanics. In the next section, we revisit the problem studied by Freund (1973). Here, in addition to the dynamic stress intensity factor history, we also try to obtain the full field analytical solution for the stresses around the crack-tip. From the full field solution, the coefficients of the higher order terms which appear in Rosakis *et al.* (1991) and Liu and Rosakis (1992) are determined for this specific problem. To demonstrate the existence of transient effects, we also study the normal traction ahead of the moving crack-tip and compare it to the equivalent traction of the K_I^d-dominant field and the field represented by the higher order transient terms. The result shows that even for a point which is relatively far away from the crack-tip, or for times very close to crack initiation, the higher order transient representation provides a very good description of the actual stress field while the K_I^d-dominant field is incapable of representing the stress field with any accuracy. In Section 3, we use the result obtained in Section 2 to interpret the experimental observations of Prakash and Clifton (1992) and to thus provide further evidence of the existence of measurable transient effects in dynamic fracture. In the process we also provide indirect evidence supporting a particular fracture criterion governing dynamic crack growth. This provides an additional example of the influence of transient effects in a new and important specimen configuration for dynamic fracture studies under very high loading rate conditions.

2 Analytical solution

2.1 Description of the analytical problem

Let $\mathcal{R}$ be an unbounded two-dimensional region occupied by an isotropic, homogeneous, linearly elastic body. The region $\mathcal{R}$ contains a straight semi-infinite crack. Let (x_1, x_2) be an orthonormal Cartesian coordinate system such that the crack occupies the entire $-\infty < x_1 \leq 0,\ x_2 = 0$, see Fig.1. Initially, the material surrounding the crack is at rest and stress free, and the crack-tip remains stationary. A planar longitudinal tension wave with a constant amplitude σ^*, propagates toward the crack and the wavefront is parallel to the crack plane. At time $t = 0$, the stress wave strikes the crack and is partially reflected and partially diffracted. The diffracted waves radiate from the crack-tip and propagate into the body. If the material occupying the body is of limited strength, then the crack will start to grow at some later time, say $t = \tau$. In order to obtain

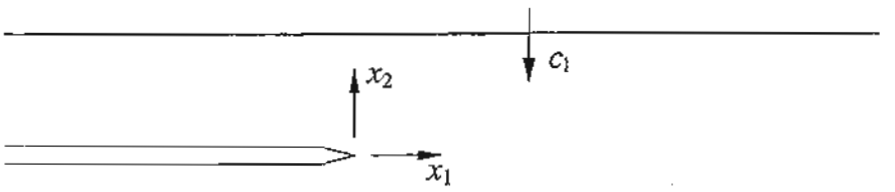

Figure 1: A semi-infinite crack loaded by a planar longitudinal wave.

the complete full field analytical solution for this transient problem, we assume that the rate of crack growth v is a constant, but we will relax this restriction in Section 3. If the deformation is assumed to be plane strain, the displacement field surrounding the crack-tip may be generated from two displacement potentials, $\phi(x_1, x_2, t)$ and $\psi(x_1, x_2, t)$, by the following relation,

$$u_\alpha(x_1, x_2, t) = \phi_{,\alpha}(x_1, x_2, t) + e_{\alpha\beta}\psi_{,\beta}(x_1, x_2, t), \tag{1}$$

where $\alpha, \beta \in \{1, 2\}$ and the summation convention has been used. $e_{\alpha\beta}$ is the two-dimensional alternator defined by

$$e_{12} = -e_{21} = 1, \quad e_{11} = e_{22} = 0.$$

The components of stress associated with this deformation can be expressed in terms of the displacement potentials as

$$\left.\begin{aligned} \sigma_{11} &= \mu\left\{\frac{c_l^2}{c_s^2}\phi_{,\alpha\alpha} - 2\phi_{,22} + 2\psi_{,12}\right\} \\ \sigma_{22} &= \mu\left\{\frac{c_l^2}{c_s^2}\phi_{,\alpha\alpha} - 2\phi_{,11} - 2\psi_{,12}\right\} \\ \sigma_{12} &= \mu\left\{2\phi_{,12} + \psi_{,22} - \psi_{,11}\right\} \end{aligned}\right\}, \tag{2}$$

where μ is the shear modulus, and c_l, c_s are the longitudinal and shear wave speeds of the elastic material, respectively.

The equation of motion in the absence of body forces and in terms of $\phi(x_1, x_2, t)$ and $\psi(x_1, x_2, t)$, reduces to

$$\left.\begin{aligned} \phi_{,\alpha\alpha}(x_1, x_2, t) - a^2\ddot{\phi}(x_1, x_2, t) &= 0 \\ \psi_{,\alpha\alpha}(x_1, x_2, t) - b^2\ddot{\psi}(x_1, x_2, t) &= 0 \end{aligned}\right\}, \tag{3}$$

where $a = 1/c_l$ and $b = 1/c_s$.

The crack faces remain traction free during the entire process, therefore the boundary conditions will be

$$\sigma_{2\alpha}(x_1, 0^{\pm}, t) = 0, \quad -\infty < x_1 < v(t-\tau)H(t-\tau), \quad \alpha \in \{1, 2\}, \quad (4)$$

where $H(\cdot)$ is the Heaviside step function.

At time $t = 0$, we can write the stress field inside the two-dimensional body as

$$\left.\begin{aligned} \sigma_{11}(x_1, x_2, 0) &= \frac{\nu\sigma^*}{1-\nu}H(x_2) \\ \sigma_{22}(x_1, x_2, 0) &= \sigma^* H(x_2) \\ \sigma_{12}(x_1, x_2, 0) &= 0 \end{aligned}\right\}, \quad (x_1, x_2) \in \mathcal{R}, \quad (5)$$

where ν is the Poisson's ratio of the elastic body.

To solve the above problem and obtain the complete full field solution, we will follow the procedure outlined by Freund (1973 and 1990), namely the method of linear superposition. As discussed by Freund, we consider the following four separate problems shown Fig.2. In problem A, the incident planar longitudinal stress wave with a constant amplitude σ^*, propagates through a body without a crack. This stress wave will induce a traction on the plane which will be occupied by the initial crack shown as the dashed lines in Fig.2. In problem B, we consider a body containing a stationary semi-infinite crack subjected to a uniform pressure on its surfaces. The magnitude of the pressure is equal to the amplitude of the plane wave considered in problem A. The combination of solutions for these two problems provides the solution for the problem of diffraction of a planar stress wave by a stationary crack. As a result of the stress wave diffraction at the crack-tip, a traction distribution is generated along the plane ahead of the crack-tip. In order to extend, the crack must in effect negate this traction distribution. Accordingly, in problem C, we study the case of the crack starting to grow with a constant speed v, at some finite delay time τ after the diffraction has occurred. During the growing process, a traction distribution will appear on the newly formed crack surface and this traction distribution will be equal but opposite to the traction distribution ahead of the crack-tip in problem B. Finally, in problem D, the crack propagates with the same constant speed v as in problem C, and a uniform pressure with the magnitude σ^* is applied

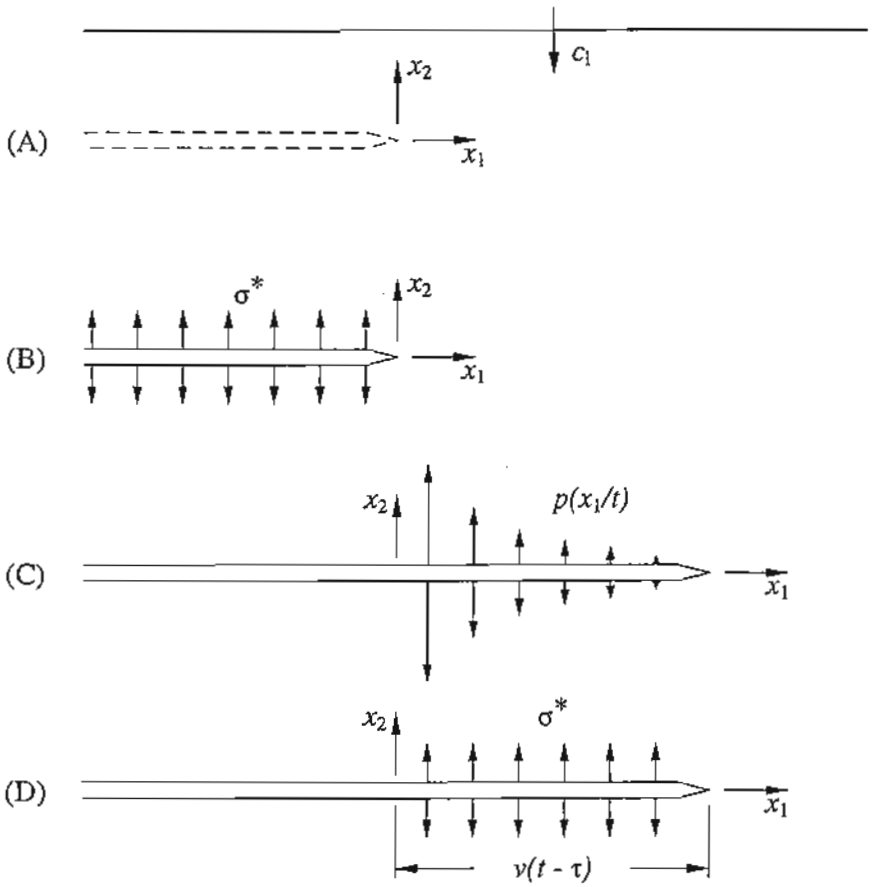

Figure 2: Schematic representation of the various boundary value problems considered in constructing the solution for constant speed crack growth under stress wave loading conditions.

on the newly created crack faces. The sum of solutions of these four problems provides the final solution for the problem we considered in this study, i.e., the one that corresponds to the case of a planar wave which strikes the crack and then, after some finite time, the crack extends at a constant speed.

In the following section, we will give the analytical results pertinent to the problems discussed above with little development. Nevertheless, besides the history of the dynamic stress intensity factor at the stationary and the moving crack-tips, which has drawn most of the attentions in previous studies, we will also provide the full field solution for the stresses surrounding the stationary and moving crack-tips. Due to length

limit, we will omit most of the details in getting those solutions, however, the reader can acquire these details from Freund (1973 and 1990), and Achenbach (1973).

2.2 The elastodynamic stress field

In this section, we study the four problems discussed in the last section separately. The solutions of these four problems will provide the final solution for our initial problem.

2.2.1 Problem A: Plane wave in an unbounded body

In this problem, we consider a planar longitudinal stress wave with a constant amplitude σ^*, which propagates in an unbounded two-dimensional region. In the Cartesian coordinate system shown in Fig.2, the wave front is parallel to the x_1-axis, and the wave propagates in the direction of negative x_2-axis. The wave speed is c_l and the moment that the wave front reaches the plane $x_2 = 0$, is designated as $t = 0$. For this problem, we can write the in plane stress components $\sigma^{(A)}_{\alpha\beta}(x_1, x_2, t)$ as follows:

$$\left.\begin{array}{rcl} \sigma^{(A)}_{11}(x_1, x_2, t) & = & \dfrac{\nu\sigma^*}{1-\nu} H(t + c_l x_2) \\ \sigma^{(A)}_{22}(x_1, x_2, t) & = & \sigma^* H(t + c_l x_2) \\ \sigma^{(A)}_{12}(x_1, x_2, t) & = & 0 \end{array}\right\}, \quad (x_1, x_2) \in \mathcal{R}. \qquad (6)$$

Once again, $H(\cdot)$ is the Heaviside step function.

2.2.2 Problem B: Stationary crack subjected to suddenly applied pressure

Let's consider the unbounded two-dimensional region $\mathcal{R}$. The Cartesiancoordinate system is chosen as in Fig.2, and the semi-infinite crack occupies the semi-infinite line of $-\infty < x_1 \leq 0$, $x_2 = 0$. For time $t < 0$, the body is stress free and at rest everywhere. At time $t = 0$, a uniformly distributed pressure with magnitude σ^*, is applied on the crack faces. From the symmetry of this loading condition, we can see that the deformation is mode-I type. Thus, we only need to consider the half

plane $\overset{+}{\mathcal{R}}$, where

$$\overset{+}{\mathcal{R}} = \{ (x_1, x_2) \mid -\infty < x_1 < \infty,\ 0 < x_2 < \infty \}.$$

Let the two displacement potentials associated with this problem be $\phi^{(B)}(x_1, x_2, t)$ and $\psi^{(B)}(x_1, x_2, t)$, then they will satisfy the equation of motion (3) in the region $\overset{+}{\mathcal{R}}$. The boundary conditions are

$$\left.\begin{aligned} &\sigma_{22}^{(B)}(x_1, 0^+, t) = -\sigma^* H(t), && -\infty < x_1 \le 0 \\ &\sigma_{12}^{(B)}(x_1, 0^+, t) = 0, && -\infty < x_1 < \infty \\ &u_2^{(B)}(x_1, 0^+, t) = 0, && 0 < x_1 < \infty \end{aligned}\right\}, \quad t > 0. \tag{7}$$

The initial conditions are

$$\left.\begin{aligned} &\phi^{(B)}(x_1, x_2, 0) = \psi^{(B)}(x_1, x_2, 0) = 0 \\ &\dot{\phi}^{(B)}(x_1, x_2, 0) = \dot{\psi}^{(B)}(x_1, x_2, 0) = 0 \end{aligned}\right\}, \quad (x_1, x_2) \in \overset{+}{\mathcal{R}}. \tag{8}$$

Meanwhile, since the displacement should be bounded throughout the region, or the mechanical energy density should be integrable, but the stress may be singular at the crack-tip, we also have

$$\int_{\mathcal{R}'} \left(\sigma_{\alpha\beta}^{(B)} \epsilon_{\alpha\beta}^{(B)} + \rho \ddot{u}_\alpha^{(B)} \dot{u}_\alpha^{(B)} \right) \mathrm{d}A < \infty, \quad \mathcal{R}' \subset \overset{+}{\mathcal{R}}. \tag{9}$$

To solve the above initial/boundary value problem, a one-side Laplace transform with respect to time t, and a two-side Laplace transform with respect to the coordinate x_1 are used. The transformed solution for the two displacement potentials can be expressed as (Freund, 1990),

$$\left.\begin{aligned} \Phi^{(B)}(\zeta, x_2, s) &= \frac{\sigma^*}{\mu} \cdot \frac{P^{(B)}(\zeta)}{s^4} e^{-s\alpha^{(B)}(\zeta) x_2} \\ \Psi^{(B)}(\zeta, x_2, s) &= \frac{\sigma^*}{\mu} \cdot \frac{Q^{(B)}(\zeta)}{s^4} e^{-s\beta^{(B)}(\zeta) x_2} \end{aligned}\right\}, \quad x_2 \in (0, \infty), \tag{10}$$

where

$$\left.\begin{aligned} P^{(B)}(\zeta) &= \frac{b^2 - 2\zeta^2}{\zeta R^{(B)}(\zeta)} \cdot \frac{F_+^{(B)}(0)}{F_+^{(B)}(\zeta)} \\ Q^{(B)}(\zeta) &= \frac{2\alpha^{(B)}(\zeta)}{R^{(B)}(\zeta)} \cdot \frac{F_+^{(B)}(0)}{F_+^{(B)}(\zeta)} \end{aligned}\right\}, \tag{11}$$

and

$$\left.\begin{aligned} R^{(\mathrm{B})}(\zeta) &= \left(b^2-2\zeta^2\right)^2+4\zeta^2\alpha^{(\mathrm{B})}(\zeta)\beta^{(\mathrm{B})}(\zeta) \\ \alpha^{(\mathrm{B})}(\zeta) &= \left(a^2-\zeta^2\right)^{1/2}, \quad \beta^{(\mathrm{B})}(\zeta) = \left(b^2-\zeta^2\right)^{1/2} \\ F_+^{(\mathrm{B})}(\zeta) &= \frac{\alpha_+^{(\mathrm{B})}(\zeta)}{(c+\zeta)S_+^{(\mathrm{B})}(\zeta)} \end{aligned}\right\}.$$

In the above expressions, appropriate branch cuts have been chosen. Also, $\alpha_+^{(\mathrm{B})}(\zeta)=(a+\zeta)^{1/2}$, $c=1/c_R$ where c_R is the Rayleigh wave speed of the elastic material, and

$$S_+^{(\mathrm{B})}(\zeta)=\exp\left\{-\frac{1}{\pi}\int_a^b \tan^{-1}\left[\frac{4\eta^2\sqrt{(\eta^2-a^2)(b^2-\eta^2)}}{(b^2-2\eta^2)^2}\right]\frac{\mathrm{d}\eta}{\eta+\zeta}\right\}.$$

The subscript + indicates that the function is analytic in the half plane Re $\zeta > -a$, and this comes from the Wiener-Hopf procedure used to solve this problem.

In order to obtain the stress field surrounding the stationary crack-tip, we need to perform the inverse transforms of those transformed stress components which can be obtained from the expressions in eqn (10). However, from the constitutive relation (2), it can be seen that the stress components are related to the second derivatives of the two displacement potentials, $\phi^{(\mathrm{B})}(x_1,x_2,t)$ and $\psi^{(\mathrm{B})}(x_1,x_2,t)$. Let $\Phi_{\alpha\beta}^{(\mathrm{B})}(\zeta,x_2,s)$ and $\Psi_{\alpha\beta}^{(\mathrm{B})}(\zeta,x_2,s)$ be the transforms of $\phi_{,\alpha\beta}^{(\mathrm{B})}(x_1,x_2,t)$ and $\psi_{,\alpha\beta}^{(\mathrm{B})}(x_1,x_2,t)$, respectively. Then, we can write that

$$\left.\begin{aligned} \Phi_{\alpha\beta}^{(\mathrm{B})}(\zeta,x_2,s) &= \frac{\sigma^*}{\mu}\cdot\frac{P_{\alpha\beta}^{(\mathrm{B})}(\zeta)}{s^2}e^{-s\alpha^{(\mathrm{B})}(\zeta)x_2} \\ \Psi_{\alpha\beta}^{(\mathrm{B})}(\zeta,x_2,s) &= \frac{\sigma^*}{\mu}\cdot\frac{Q_{\alpha\beta}^{(\mathrm{B})}(\zeta)}{s^2}e^{-s\beta^{(\mathrm{B})}(\zeta)x_2} \end{aligned}\right\}, \quad x_2\in(0,\infty), \tag{12}$$

where

$$\left.\begin{aligned} P_{11}^{(\mathrm{B})}(\zeta) &= \zeta^2 P^{(\mathrm{B})}(\zeta) \\ P_{22}^{(\mathrm{B})}(\zeta) &= \left(a^2-\zeta^2\right)P^{(\mathrm{B})}(\zeta) \\ P_{12}^{(\mathrm{B})}(\zeta) &= -\zeta\alpha^{(\mathrm{B})}(\zeta)P^{(\mathrm{B})}(\zeta) \end{aligned}\right\}, \quad \left.\begin{aligned} Q_{11}^{(\mathrm{B})}(\zeta) &= \zeta^2 Q^{(\mathrm{B})}(\zeta) \\ Q_{22}^{(\mathrm{B})}(\zeta) &= \left(b^2-\zeta^2\right)Q^{(\mathrm{B})}(\zeta) \\ Q_{12}^{(\mathrm{B})}(\zeta) &= -\zeta\beta^{(\mathrm{B})}(\zeta)Q^{(\mathrm{B})}(\zeta) \end{aligned}\right\}.$$

Several observations can be made at this point: i) $P_{11}^{(\mathrm{B})}(\zeta)$ and $P_{12}^{(\mathrm{B})}(\zeta)$ are analytic in the strip $-a < \mathrm{Re}\ \zeta < a$; $P_{22}^{(\mathrm{B})}(\zeta)$ is analytic in the strip $-a < \mathrm{Re}\ \zeta < a$, but has a simple pole at $\zeta = 0$; ii) $Q_{\alpha\beta}^{(\mathrm{B})}(\zeta)$ are analytic the strip $-b < \mathrm{Re}\ \zeta < a$, where $\alpha, \beta \in \{1, 2\}$; iii) All singularities and branch cuts lie along the real axis.

By using the Cagniard-de Hoop technique to the transformed second derivatives in eqn (12) and by using the above observations for the regions of analyticity for each function, the second derivatives of the displacement potential associated with the longitudinalwave, $\phi^{(\mathrm{B})}(x_1, x_2, t)$, can be expressed as (see Appendix)

$$\left.\begin{aligned}
\phi^{(\mathrm{B})}_{,11}(x_1, x_2, t) &= \frac{\sigma^*}{\pi\mu} \int_{ar}^{t} \mathrm{Im}\left\{ P_{11}^{(\mathrm{B})}(\zeta_l^{(\mathrm{B})}) \frac{\partial \zeta_l^{(\mathrm{B})}}{\partial \tau} \right\} \mathrm{d}\tau \cdot H(t - ar) \\
\phi^{(\mathrm{B})}_{,22}(x_1, x_2, t) &= \frac{\sigma^*}{\pi\mu} \int_{-\omega_l^*}^{x_1} \mathrm{Im}\left\{ \zeta_l^{(\mathrm{B})*} P_{22}^{(\mathrm{B})}(\zeta_l^{(\mathrm{B})*}) \frac{\partial \zeta_l^{(\mathrm{B})*}}{\partial t} \right\} \mathrm{d}x_1^* \cdot H(t - ar) \\
\phi^{(\mathrm{B})}_{,12}(x_1, x_2, t) &= \frac{\sigma^*}{\pi\mu} \int_{ar}^{t} \mathrm{Im}\left\{ P_{12}^{(\mathrm{B})}(\zeta_l^{(\mathrm{B})}) \frac{\partial \zeta_l^{(\mathrm{B})}}{\partial \tau} \right\} \mathrm{d}\tau \cdot H(t - ar)
\end{aligned}\right\}, \tag{13}$$

where

$$\zeta_l^{(\mathrm{B})}(x_1, x_2, t) = -\frac{t}{r}\cos\theta + i\sqrt{\frac{t^2}{r^2} - a^2}\sin\theta, \tag{14}$$

and (r, θ) are the polar coordinates centered at the stationary crack-tip. $\zeta_l^{(\mathrm{B})*}(x_1^*, x_2, t)$ has the same form as that in eqn (14) except that x_1 should be replaced by x_1^*. Also

$$\omega_l^* = \left(\frac{t^2}{a^2} - x_2^2 \right)^{1/2}.$$

Similarly, the second derivatives of the displacement potential associated with the transverse wave, $\psi^{(\mathrm{B})}(x_1, x_2, t)$, can be expressed as (see Appendix)

$$\left.\begin{aligned}
\psi^{(\mathrm{B})}_{,\alpha\beta}(x_1, x_2, t) = \frac{\sigma^*}{\pi\mu} \Bigg\{ &\int_{br}^{t} \mathrm{Im}\left[Q_{\alpha\beta}^{(\mathrm{B})}(\zeta_s^{(\mathrm{B})}) \frac{\partial \zeta_s^{(\mathrm{B})}}{\partial \tau} \right] \mathrm{d}\tau \cdot H(t - br) \\
&+ \int_{a}^{\lambda^{(\mathrm{B})}(\theta)} \mathrm{Im}\left[Q_{\alpha\beta}^{(\mathrm{B})+}(\eta) \right] h^{(\mathrm{B})}(\eta) \mathrm{d}\eta \cdot H(\theta - \theta_{\mathrm{H}}^{(\mathrm{B})}) \Bigg\}
\end{aligned}\right\}, \tag{15}$$

where $\alpha, \beta \in \{1, 2\}$, and

$$\zeta_s^{(\mathrm{B})}(x_1, x_2, t) = -\frac{t}{r}\cos\theta + i\sqrt{\frac{t^2}{r^2} - b^2}\sin\theta. \tag{16}$$

In addition, in eqn (15), $\lambda^{(B)}(\theta) = -b\cos\theta$, and $\theta_H^{(B)} = \pi - \cos^{-1}(a/b)$. Also,

$$h^{(B)}(\eta) = H\left(t - [\beta^{(B)}(\eta)x_2 - \eta x_1]\right), \quad a < \eta \leq \lambda^{(B)}(\theta).$$

It should be noted that the second part of the right-hand side in eqn (15) provides information inside the head wave region.

By substituting eqns (13) and (15) into the constitutive relation (2), we can get the stress field surrounding the stationary crack-tip for problem B. As an input to problem C, we need to know the normal traction $\sigma_+^{(B)}(x_1, t)$, ahead of the stationary crack-tip in problem B. It can be shown that (Freund, 1990)

$$\sigma_+^{(B)}(x_1, t) = \frac{\sigma^*}{\pi}\left\{\int_{ax_1}^{t} \mathrm{Im}\left[\frac{F_+^{(B)}(0)}{F_+^{(B)+}(-\eta/x_1)}\right]\frac{\mathrm{d}\eta}{\eta}\right\} \cdot H(t - ax_1), \qquad (17)$$

or $\sigma_+^{(B)}(x_1, t)$ may also be expressed as

$$p(u) = \frac{\sigma^*}{\pi}\left\{\int_{a}^{1/u} \mathrm{Im}\left[\frac{F_+^{(B)}(0)}{F_+^{(B)+}(-\omega)}\right]\frac{\mathrm{d}\omega}{\omega}\right\} \cdot H\left(\frac{1}{u} - a\right), \qquad (18)$$

where $u = x_1/t$. It must be pointed out that the normal traction ahead of the stationary crack-tip, $\sigma_+^{(B)}(x_1, t)$, or $p(x_1/t)$, is a homogeneous function of x_1 and t of degree zero. Finally, the dynamic stress intensity factor at the stationary crack-tip for problem B is

$$K_I^{d(B)}(t) = \frac{2\sigma^*}{1-\nu}\sqrt{\frac{(1-2\nu)c_l t}{\pi}}, \quad t > 0. \qquad (19)$$

2.2.3 Problem C: Moving crack with varying traction applied on its new surface

In this problem, we study the semi-infinite crack configuration considered in problem B. At time $t = \tau$, the crack starts to extend with a constant speed v. At the same time, a compressive normal traction of magnitude of $p(x_1/t)$, given in (18), is applied on the newly created crack faces, $0 < x_1 < v(t - \tau)$. Since the traction distribution (18) has the property of homogeneity, any fixed stress level in the scattered field radiates out along the x_1-axis at constant speed. As a result of this observation, the solution for problem C can be further generated by the so-called fundamental solution (Freund, 1990).

Consider the region $\mathcal{R}$ and a semi-infinite crack lying along the entire negative x_1-axis in the Cartesian coordinate system, (x_1, x_2). As time $t < 0$, the body is stress free and at rest everywhere. At $t = 0$, a pair of concentrated forces $p(t)$, of the form,

$$p(t) = p_0 + p_1 t,$$

where p_0 and p_1 are constants, is applied at the crack-tip and tends to open the crack. At the same time, the crack begins to propagate with a constant speed v. Meanwhile, the concentrated force $p(t)$ also propagates with a constant velocity $u < v$ toward the moving crack-tip. Let $\phi^{(\mathrm{F})}(x_1, x_2, t)$ and $\psi^{(\mathrm{F})}(x_1, x_2, t)$ be the two displacement potentials for the fundamental problem. Then, $\phi^{(\mathrm{F})}(x_1, x_2, t)$ and $\psi^{(\mathrm{F})}(x_1, x_2, t)$ will satisfy the equation of motion (3) and the same initial conditions (8). The boundary conditions are

$$\left.\begin{aligned} &\sigma_{22}^{(\mathrm{F})}(x_1, 0^+, t) = -(p_0 + p_1 t)\,\delta(x_1 - ut)H(t), && -\infty < x_1 \le vt \\ &\sigma_{12}^{(\mathrm{F})}(x_1, 0^+, t) = 0, && -\infty < x_1 < \infty \\ &u_2^{(\mathrm{F})}(x_1, 0^+, t) = 0, && vt < x_1 < \infty \end{aligned}\right\}, \tag{20}$$

where $\delta(\cdot)$ is the Dirac delta function. By defining the moving coordinates (ξ_1, ξ_2) through $\xi_1 = x_1 - vt$, $\xi_2 = x_2$, and applying the Laplace transforms with respect to t and ξ_1, the solutions in the transformed plane will be

$$\left.\begin{aligned} \Phi^{(\mathrm{F})}(\zeta, \xi_2, s) &= \frac{p_0}{\mu} \cdot \frac{P_0(\zeta)}{s^3} e^{-s\alpha(\zeta)\xi_2} - \frac{p_1}{\mu} \cdot \frac{P_1(\zeta)}{s^4} e^{-s\alpha(\zeta)\xi_2} \\ \Psi^{(\mathrm{F})}(\zeta, \xi_2, s) &= \frac{p_0}{\mu} \cdot \frac{Q_0(\zeta)}{s^3} e^{-s\beta(\zeta)\xi_2} - \frac{p_1}{\mu} \cdot \frac{Q_1(\zeta)}{s^4} e^{-s\beta(\zeta)\xi_2} \end{aligned}\right\}, \xi_2 \in (0, \infty), \tag{21}$$

where

$$\left.\begin{aligned} P_0(\zeta) &= \frac{w\{\beta^2(\zeta) - \zeta^2\}}{(\zeta - w)R(\zeta)} \cdot \frac{F_+(w)}{F_+(\zeta)} \\ Q_0(\zeta) &= \frac{2w\zeta\alpha(\zeta)}{(\zeta - w)R(\zeta)} \cdot \frac{F_+(w)}{F_+(\zeta)} \end{aligned}\right\}, \tag{22}$$

and

$$\left.\begin{aligned} P_1(\zeta) &= \frac{w^2\{\beta^2(\zeta) - \zeta^2\}}{R(\zeta)F_+(\zeta)} \cdot \left[\frac{F_+(w)}{\zeta - w}\right]' \\ Q_1(\zeta) &= \frac{2w^2\zeta\alpha(\zeta)}{R(\zeta)F_+(\zeta)} \cdot \left[\frac{F_+(w)}{\zeta - w}\right]' \end{aligned}\right\}. \tag{23}$$

In the above expressions, prime denotes the derivative with respect to the argument w, where $w = 1/(v-u)$, and

$$
\begin{aligned}
R(\zeta) &= 4\zeta^2\alpha(\zeta)\beta(\zeta) + \left\{\beta^2(\zeta) - \zeta^2\right\}^2 , \\
\alpha(\zeta) &= \left(a^2 - \zeta^2 + \frac{a^2\zeta^2}{h^2} - \frac{2a^2\zeta}{h}\right)^{1/2} , \\
\beta(\zeta) &= \left(b^2 - \zeta^2 + \frac{b^2\zeta^2}{h^2} - \frac{2b^2\zeta}{h}\right)^{1/2} , \\
F_+(\zeta) &= \frac{\alpha_+(\zeta)}{(c_- + \zeta)\, S_+(\zeta)} , \quad \alpha_+(\zeta) = \left\{a + \left(1 - \frac{a}{h}\right)\zeta\right\}^{1/2} , \\
S_+(\zeta) &= \exp\left\{-\frac{1}{\pi}\int_{a_-}^{b_-} \tan^{-1}\left[\frac{4\eta^2\beta(-\eta)|\alpha(-\eta)|}{\left[\beta^2(-\eta) - \eta^2\right]^2}\right]\frac{\mathrm{d}\eta}{\eta + \zeta}\right\} ,
\end{aligned}
$$

in which $h = 1/v$. Also,

$$
a_\pm = \frac{a}{1 \pm a/h}, \quad b_\pm = \frac{b}{1 \pm b/h}, \quad c_\pm = \frac{c}{1 \pm c/h}.
$$

Similar to the procedure used in problem B, by defining

$$
\left.
\begin{aligned}
P_{11}^{(k)}(\zeta) &= \zeta^2 P_k(\zeta) \\
P_{22}^{(k)}(\zeta) &= \alpha^2(\zeta) P_k(\zeta) \\
P_{12}^{(k)}(\zeta) &= -\zeta\alpha(\zeta) P_k(\zeta)
\end{aligned}
\right\}, \qquad
\left.
\begin{aligned}
Q_{11}^{(k)}(\zeta) &= \zeta^2 Q_k(\zeta) \\
Q_{22}^{(k)}(\zeta) &= \beta^2(\zeta) Q_k(\zeta) \\
Q_{12}^{(k)}(\zeta) &= -\zeta\beta(\zeta) Q_k(\zeta)
\end{aligned}
\right\},
$$

where $k \in \{0, 1\}$, the second derivatives of the displacement potential, $\phi^{(\mathrm{F})}(\xi_1, \xi_2, t)$, can be expressed as

$$
\left.
\begin{aligned}
\phi^{(\mathrm{F})}_{l\alpha\beta}(\xi_1, \xi_2, t) = \frac{p_0}{\pi\mu}\mathrm{Im}\left\{P^{(0)}_{\alpha\beta}(\zeta_l)\frac{\partial\zeta_l}{\partial t}\right\} \cdot H\left(t - \omega_l(r_l, \theta_l)\right) \\
- \frac{p_1}{\pi\mu}\int_{\omega_l(r_l,\theta_l)}^{t} \mathrm{Im}\left\{P^{(1)}_{\alpha\beta}(\zeta_l)\frac{\partial\zeta_l}{\partial\tau}\right\}\mathrm{d}\tau \cdot H\left(t - \omega_l(r_l, \theta_l)\right)
\end{aligned}
\right\}, \quad (24)
$$

where α, $\beta \in \{1,2\}$, and

$$\left.\begin{aligned}\zeta_l(\xi_1,\xi_2,t) &= -\left(\frac{t}{r_l} - \frac{a_- - a_+}{2}\cos\theta_l\right)\cos\theta_l - \frac{a_- - a_+}{2} \\ &\quad + i\left\{\left(\frac{t}{r_l} - \frac{a_- - a_+}{2}\cos\theta_l\right)^2 - \left(\frac{a_- + a_+}{2}\right)^2\right\}^{1/2}\sin\theta_l \\ \omega_l(r_l,\theta_l) &= r_l\left(\frac{a_- - a_+}{2}\cos\theta_l + \frac{a_- + a_+}{2}\right)\end{aligned}\right\}.$$

The second derivative of the displacement potential, $\psi^{(\mathrm{F})}(\xi_1,\xi_2,t)$, can be expressed as

$$\left.\begin{aligned}\psi^{(\mathrm{F})}_{,\alpha\beta}(\xi_1,\xi_2,t) &= \frac{p_0}{\pi\mu}\left\{\mathrm{Im}\left[Q^{(0)}_{\alpha\beta}(\zeta_s)\frac{\partial\zeta_s}{\partial t}\right]\cdot H\left(t-\omega_s(r_s,\theta_s)\right)\right. \\ &\quad \left. + \int_{a_+}^{\lambda(\theta_s)}\left[\mathrm{Im}\left(Q^{(0)+}_{\alpha\beta}(\eta)\right)d(\eta)\right]\mathrm{d}\eta\cdot H\left(\theta_s-\theta_{\mathrm{H}}\right)\right\} \\ &\quad - \frac{p_1}{\pi\mu}\left\{\int_{\omega_s(r_s,\theta_s)}^{t}\mathrm{Im}\left[Q^{(1)}_{\alpha\beta}(\zeta_s)\frac{\partial\zeta_s}{\partial\tau}\right]\mathrm{d}\tau\cdot H\left(t-\omega_s(r_s,\theta_s)\right)\right. \\ &\quad \left. + \int_{a_+}^{\lambda(\theta_s)}\left[\mathrm{Im}\left(Q^{(1)+}_{\alpha\beta}(\eta)\right)h(\eta)\right]\mathrm{d}\eta\cdot H\left(\theta_s-\theta_{\mathrm{H}}\right)\right\}\end{aligned}\right\}, \quad (25)$$

where α, $\beta \in \{1,2\}$. In eqn (25),

$$\left.\begin{aligned}\zeta_s(\xi_1,\xi_2,t) &= -\left(\frac{t}{r_s} - \frac{b_- - b_+}{2}\cos\theta_s\right)\cos\theta_s - \frac{b_- - b_+}{2} \\ &\quad + i\left\{\left(\frac{t}{r_s} - \frac{b_- - b_+}{2}\cos\theta_s\right)^2 - \left(\frac{b_- + b_+}{2}\right)^2\right\}^{1/2}\sin\theta_s \\ \omega_s(r_s,\theta_s) &= r_s\left(\frac{b_- - b_+}{2}\cos\theta_s + \frac{b_- + b_+}{2}\right)\end{aligned}\right\},$$

and

$$\left.\begin{aligned}\lambda(\theta_s) &= -\left(\frac{b_- + b_+}{2}\cos\theta_s + \frac{b_- - b_+}{2}\right) \\ \theta_{\mathrm{H}} &= \pi - \cos^{-1}\left(\frac{2a_+}{b_- + b_+} + \frac{b_- - b_+}{b_- + b_+}\right)\end{aligned}\right\}.$$

Also,

$$\left.\begin{aligned}d(\eta) &= \delta\left(t - [\beta(\eta)\xi_2 - \eta\xi_1]\right) \\ h(\eta) &= H\left(t - [\beta(\eta)\xi_2 - \eta\xi_1]\right)\end{aligned}\right\}, \quad a_+ \le \eta \le \lambda(\theta_s).$$

In eqns (24) and (25), $(r_{l,s}, \theta_{l,s})$ are two scaled polar coordinate systems defined by

$$r_{l,s} = \left\{\xi_1^2 + \alpha_{l,s}^2 \xi_2^2\right\}^{1/2}, \quad \theta_{l,s} = \tan^{-1} \frac{\alpha_{l,s}\xi_2}{\xi_1},$$

where

$$\alpha_l = \left(1 - \frac{a^2}{h^2}\right)^{1/2}, \quad \alpha_s = \left(1 - \frac{b^2}{h^2}\right)^{1/2}.$$

The components of stress field for the fundamental problem can be obtained by using the constitutive relation (2).

Returning to problem C, let $q^{(\mathrm{F})}(\xi_1, \xi_2, t; w)$ be any element of the fundamental solution, such as the stress components, particle velocity, etc., and the dependence of the fundamental solution on the parameter w is made explicitly here. Following the analysis given by Freund (1973 and 1990), the corresponding element $q^{(\mathrm{C})}(\xi_1, \xi_2, t)$ for problem C will be given by

$$q^{(\mathrm{C})}(\xi_1, \xi_2, t) = \int_h^{h^*} q^{(\mathrm{F})}\left(\xi_1, \xi_2, \frac{\tau}{h}(h^* - w); w\right) \frac{p^*(w)}{w^2} \mathrm{d}w, \qquad (26)$$

where $h^* = ht/\tau$, $p^*(w) = p((vw-1)/w)$. It should be pointed out that in eqn (26), quantities p_0 and p_1 that appear in the fundamental solutions have been changed to $\tau w/h$ and 1, respectively. Finally, the dynamic stress intensity factor at the moving crack-tip in problem C is given by

$$K_I^{d(\mathrm{C})}(t) = 2\sigma^* k(v)\sqrt{\frac{2}{\pi}}\left\{\frac{\sqrt{2c_l t(1-2\nu)}}{2(1-\nu)} - \sqrt{v(t-\tau)}\right\}, \quad t > \tau, \qquad (27)$$

where $k(v)$ is a universal function of the crack-tip speed given by

$$k(v) = \frac{1 - c/h}{S_+(h)\sqrt{1 - a/h}}, \quad h = \frac{1}{v}. \qquad (28)$$

2.2.4 Problem D: Moving crack with uniform pressure applied on its new surface

Similar to problem C, we study the semi-infinite crack configuration considered in problem B. At time $t = \tau$, the crack starts to extend with a

constant speed v. However, at the same time, a uniform pressure of magnitude of σ^*, is applied on the newly created crack faces, $0 < x_1 < v(t-\tau)$. Let $\phi^{(\mathrm{D})}(x_1, x_2, t)$ and $\psi^{(\mathrm{D})}(x_1, x_2, t)$ be the displacement potentials of this problem. For analysis convenience, consider that the crack-tip starts to extend at $t = 0$ and obtain the displacement potentials for this new problem, denoted as problem M. Therefore, $\phi^{(\mathrm{M})}(x_1, x_2, t)$ and $\psi^{(\mathrm{M})}(x_1, x_2, t)$ satisfy the equation of motion (3), and the boundary conditions are

$$\left.\begin{aligned} \sigma_{22}^{(\mathrm{M})}(x_1, 0^+, t) &= -\sigma^* H(x_1) H(vt - x_1) H(t), && -\infty < x_1 \le vt \\ \sigma_{12}^{(\mathrm{M})}(x_1, 0^+, t) &= 0, && -\infty < x_1 < \infty \\ u_2^{(\mathrm{M})}(x_1, 0^+, t) &= 0, && vt < x_1 < \infty \end{aligned}\right\}. \quad (29)$$

In the moving coordinate system (ξ_1, ξ_2), after the Laplace transforms are applied, the solutions are

$$\left.\begin{aligned} \Phi^{(\mathrm{M})}(\zeta, \xi_2, s) &= \frac{\sigma^*}{\mu} \cdot \frac{P^{(\mathrm{M})}(\zeta)}{s^4} e^{-s\alpha(\zeta)\xi_2} \\ \Psi^{(\mathrm{M})}(\zeta, \xi_2, s) &= \frac{\sigma^*}{\mu} \cdot \frac{Q^{(\mathrm{M})}(\zeta)}{s^4} e^{-s\beta(\zeta)\xi_2} \end{aligned}\right\}, \quad \xi_2 \in (0, \infty), \quad (30)$$

where

$$\left.\begin{aligned} P^{(\mathrm{M})}(\zeta) &= \frac{\beta^2(\zeta) - \zeta^2}{(\zeta - h)R(\zeta)} \cdot \frac{F_+(h)}{F_+(\zeta)} \\ Q^{(\mathrm{M})}(\zeta) &= \frac{2\zeta\alpha(\zeta)}{(\zeta - h)R(\zeta)} \cdot \frac{F_+(h)}{F_+(\zeta)} \end{aligned}\right\}, \quad (31)$$

where all quantities that appear in the above expressions have been given in the solutions for problem C. By defining

$$\left.\begin{aligned} P_{11}^{(\mathrm{M})}(\zeta) &= \zeta^2 P^{(\mathrm{M})}(\zeta) \\ P_{22}^{(\mathrm{M})}(\zeta) &= \alpha^2(\zeta) P^{(\mathrm{M})}(\zeta) \\ P_{12}^{(\mathrm{M})}(\zeta) &= -\zeta\alpha(\zeta) P^{(\mathrm{M})}(\zeta) \end{aligned}\right\}, \quad \left.\begin{aligned} Q_{11}^{(\mathrm{M})}(\zeta) &= \zeta^2 Q^{(\mathrm{M})}(\zeta) \\ Q_{22}^{(\mathrm{M})}(\zeta) &= \beta^2(\zeta) Q^{(\mathrm{M})}(\zeta) \\ Q_{12}^{(\mathrm{M})}(\zeta) &= -\zeta\beta(\zeta) Q^{(\mathrm{M})}(\zeta) \end{aligned}\right\},$$

the second derivatives of $\phi^{(\mathrm{M})}(\xi_1, \xi_2, t)$ and $\psi^{(\mathrm{M})}(\xi_1, \xi_2, t)$ will be

$$\phi_{,\alpha\beta}^{(\mathrm{M})}(\xi_1, \xi_2, t) = \frac{\sigma^*}{\pi\mu} \int_{\omega_l(r_l, \theta_l)}^{t} \mathrm{Im}\left\{ P_{\alpha\beta}^{(\mathrm{M})}(\zeta_l) \frac{\partial \zeta_l}{\partial \tau} \right\} \mathrm{d}\tau \cdot H\left(t - \omega_l(r_l, \theta_l)\right), \quad (32)$$

and

$$\psi^{(\mathrm{M})}_{,\alpha\beta}(\xi_1,\xi_2,t) = \frac{\sigma^*}{\pi\mu}\left\{\begin{array}{l}\displaystyle\int_{\omega_s(r_s,\theta_s)}^{t} \mathrm{Im}\left[Q^{(\mathrm{M})}_{\alpha\beta}(\zeta_s)\frac{\partial\zeta_s}{\partial\tau}\right]\mathrm{d}\tau\cdot H\left(t-\omega_s(r_s,\theta_s)\right) \\ \displaystyle+\int_{a_+}^{\lambda(\theta_s)}\left[\mathrm{Im}\left(Q^{(\mathrm{M})+}_{\alpha\beta}(\eta)\right)h(\eta)\right]\mathrm{d}\eta\cdot H\left(\theta_s-\theta_{\mathrm{H}}\right)\end{array}\right\}. \tag{33}$$

For problem D, we can get

$$\left.\begin{array}{l}\phi^{(\mathrm{D})}_{,\alpha\beta}(\xi_1,\xi_2,t) = \phi^{(\mathrm{M})}_{,\alpha\beta}(\xi_1,\xi_2,t-\tau) \\ \psi^{(\mathrm{D})}_{,\alpha\beta}(\xi_1,\xi_2,t) = \psi^{(\mathrm{M})}_{,\alpha\beta}(\xi_1,\xi_2,t-\tau)\end{array}\right\}. \tag{34}$$

The components of stress can be obtained from the constitutive relation (2). The dynamic stress intensity factor at the moving crack-tip in problem D, is given by

$$K_I^{d(\mathrm{D})}(t) = 2\sigma^* k(v)\sqrt{\frac{2v(t-\tau)}{\pi}}, \quad t>\tau. \tag{35}$$

Up to this point, we have obtained the analytical full field solution for each problem. Returning to our original problem which corresponds to a planar longitudinal stress wave of constant amplitude σ^* which strikes a semi-infinite crack, and after some time τ, the crack extends at a constant speed v, we can construct the final solution. For $0<t\le\tau$, the solution is given by the sum of problems A and B. For $t>\tau$, the solution is given by the sum of all four problems. Particularly, the dynamic stress intensity factors at the stationary and moving crack-tips are

$$K_I^d(t) = \left\{\begin{array}{ll}\dfrac{2\sigma^*}{1-\nu}\sqrt{\dfrac{(1-2\nu)c_l t}{\pi}}, & 0<t\le\tau\ , \\ \dfrac{2\sigma^* k(v)}{1-\nu}\sqrt{\dfrac{(1-2\nu)c_l t}{\pi}}, & t>\tau\ .\end{array}\right. \tag{36}$$

It is clear from eqn (36) that for an unbounded body under time-independent loading conditions, the dynamic stress intensity factor at the running crack-tip can be expressed as a universal function of instantaneous crack-tip speed multiplied by the equilibrium stress intensity factor for the given applied loading and the instantaneous amount of crack growth. It should be pointed out that the sum of problems B and C will give the

solution for the problem studied by Ravi-Chandar and Knauss (1982) and analyzed by Ma and Freund (1986). However, since the problem is no longer self-similar, the dynamic stress intensity factor at the moving crack-tip corresponding to this problem will not have the property stated above.

2.3 Higher order transient asymptotic representation of the elastodynamic field surrounding the moving crack-tip

In the previous section, we have derived the full field analytical solution for the problem stated in Section 2.1. This solution has considered the transient nature of the problem. As one can see that the expressions for the solution are complicated. In order to use the solution in comparison with experimental observations, one is interested in the asymptotic structure of this elastodynamic field, or the field very close to the moving crack-tip. Recently, Freund and Rosakis (1992) and Liu and Rosakis (1992) have developed the structure of the higher order transient asymptotic representation for the stress field around a transiently extending crack-tip in homogeneous and isotropic linear elastic materials. Their asymptotic representation involves coefficients which are complicated functions of time that cannot be completely determined by the asymptotic analysis. The crack problem under consideration here is highly transient. As such it is a good candidate to be used for obtaining the coefficients of the higher order transient asymptotic representation of the elastodynamic field surrounding the moving crack-tip. A comparison of the transient expansion with the actual full field solution will give us an indication of how well this transient asymptotic representation describes the actual field.

To obtain the asymptotic expansion of the elastodynamic field derived in the previous section, we consider the quantity $\phi_{,\alpha\alpha}(\xi_1, \xi_2, t)$. For problem A, as $t > 0$,

$$\phi^{(A)}_{,\alpha\alpha}(\xi_1, 0^+, t) = \frac{\sigma^*}{\mu} \cdot \frac{1-2\nu}{2(1-\nu)}. \tag{37}$$

In problem B, by expanding the quantity $\phi^{(B)}_{,\alpha\alpha}(x_1, 0^+, t)$ into a power

series of ξ_1 for finite $t > \tau$, where $x_1 = \xi_1 + v(t-\tau)$, we get

$$\phi_{,11}^{(B)}(\xi_1 + v(t-\tau), 0^+, t) = \frac{\sigma^*}{\mu} \cdot \frac{1}{\pi\sqrt{1-\nu}} \Omega_1^{(B)}(t) + O(\xi_1), \tag{38}$$

as $\xi_1 \to 0^+$, where

$$\left.\begin{aligned} \Omega_1^{(B)}(t) = \int_a^b & \frac{a^2(\eta-c)(b^2-2\eta^2)^3 S_+^{(B)}(-\eta)}{\eta\sqrt{b(\eta-a)}\left\{(b^2-2\eta^2)^4 + 16\eta^4(\eta^2-a^2)(b^2-\eta^2)\right\}} \mathrm{d}\eta \\ + \int_b^{\frac{ht}{t-\tau}} & \frac{a^2(\eta-c)(b^2-2\eta^2) S_+^{(B)}(-\eta)}{\eta\sqrt{b(\eta-a)}\left\{(b^2-2\eta^2)^2 - 4\eta^2\sqrt{\eta^2-a^2}\sqrt{\eta^2-b^2}\right\}} \mathrm{d}\eta \end{aligned}\right\},$$

and the function $S_+^{(B)}(\zeta)$ has been defined in Section 2.2.2.

For the fundamental problem, it can be shown that

$$\left.\begin{aligned} \phi_{,\alpha\alpha}^{(F)}(\xi_1, 0^+, t) \;=\; & \frac{(1-\alpha_l^2)(1+\alpha_s^2)}{\mu D(v)} \left\{ \frac{K_I^{d(F)}(t;w)}{\sqrt{2\pi\xi_1}} \right. \\ & -\frac{1}{\pi}\sqrt{\frac{a_-}{a}} \left[\left(\omega_0(v) + \frac{w}{h}\right) \left(p_0 \frac{hwF_+(w)}{t^{3/2}} + 2p_1 \frac{hw^2 F_+'(w)}{t^{1/2}} \right) \right. \\ & \left.\left. +2p_1 \frac{w^2 F_+(w)}{t^{1/2}} \right] \xi_1^{1/2} + O(\xi_1^{3/2}) \right\} \cdot H(t - a_-\xi_1) \end{aligned}\right\}, \tag{39}$$

as $\xi_1 \to 0^+$, where

$$\omega_0(v) = \frac{c_-}{h} - \frac{a_-}{2h} - \frac{4\alpha_s^2}{1+\alpha_s^2} + R_0(v) + S_0(v),$$

and

$$\left.\begin{aligned} R_0(v) \;&=\; \frac{4}{D(v)} \left\{ \left(1 - \alpha_s^4\right) - \frac{\alpha_l^2 + \alpha_s^2 - 2\alpha_l^2\alpha_s^2}{\alpha_l\alpha_s} \right\} \\ S_0(v) \;&=\; -\frac{1}{\pi h} \int_{a_-}^{b_-} \tan^{-1}\left[\frac{4\eta^2\beta(-\eta)|\alpha(-\eta)|}{\left[\beta^2(-\eta) - \eta^2\right]^2} \right] \mathrm{d}\eta \\ D(v) \;&=\; 4\alpha_l\alpha_s - \left(1+\alpha_s^2\right)^2 \end{aligned}\right\}.$$

From this result, as $t > \tau$, we can get the corresponding expansion for problem C by using relation (26). After some manipulations and using

the property of the Heaviside function in (39), it can be shown that

$$\left.\begin{aligned}\phi_{,\alpha\alpha}^{(\mathrm{C})}(\xi_1,0^+,t) &= \frac{(1-\alpha_l^2)(1+\alpha_s^2)}{D(v)}\cdot\frac{K_I^{d(\mathrm{C})}(t)}{\mu\sqrt{2\pi\xi_1}} \\ &+\frac{\sigma^*}{\mu}\cdot\frac{2(1-\alpha_l^2)(1+\alpha_s^2)}{D(v)}\cdot\sqrt{\frac{h}{b}}\cdot\frac{k(v)\Omega_2^{(\mathrm{C})}(t)}{\pi}\sqrt{\frac{\xi_1}{c_s\tau}}+O(\xi_1^{3/2})\end{aligned}\right\}, \quad (40)$$

as $\xi_1 \to 0^+$, where $K_I^{d(\mathrm{C})}(t)$ has been given in eqn (27) and

$$\Omega_2^{(\mathrm{C})}(t)=\frac{\sqrt{2(1-2\nu)}}{2(1-\nu)}\sqrt{\frac{h}{a}}\cdot\frac{\omega_0(v)}{\sqrt{t/\tau}}-\frac{\omega_0(v)+1}{\sqrt{t/\tau-1}}.$$

For problem D, it can be shown that as $t > \tau$,

$$\left.\begin{aligned}\phi_{,\alpha\alpha}^{(\mathrm{D})}(\xi_1,0^+,t) &= \frac{(1-\alpha_l^2)(1+\alpha_s^2)}{D(v)}\cdot\frac{K_I^{d(\mathrm{D})}(t)}{\mu\sqrt{2\pi\xi_1}} \\ &+\frac{\sigma^*}{\mu}\cdot\frac{2(1-\alpha_l^2)(1+\alpha_s^2)}{D(v)}\cdot\sqrt{\frac{h}{b}}\cdot\frac{k(v)\Omega_2^{(\mathrm{D})}(t)}{\pi}\sqrt{\frac{\xi_1}{c_s\tau}}+O(\xi_1^{3/2})\end{aligned}\right\}, \quad (41)$$

as $\xi_1 \to 0^+$, where $K_I^{d(\mathrm{D})}(t)$ has been given in eqn (35) and

$$\Omega_2^{(\mathrm{D})}(t)=\frac{\omega_0(v)+1}{\sqrt{t/\tau-1}}.$$

Finally, by superposing the above asymptotic expressions for the four constituent problems, the asymptotic representation of the quantity $\phi_{,\alpha\alpha}(\xi_1,0^+,t)$ of our original problem near the extending crack-tip is

$$\left.\begin{aligned}\phi_{,\alpha\alpha}(\xi_1,0^+,t) &= \frac{(1-\alpha_l^2)(1+\alpha_s^2)}{D(v)}\cdot\frac{K_I^d(t)}{\mu\sqrt{2\pi\xi_1}}+\frac{\sigma^*}{\mu}\Omega_1(t) \\ &+\frac{\sigma^*}{\mu}\cdot\frac{2(1-\alpha_l^2)(1+\alpha_s^2)}{D(v)}\cdot\sqrt{\frac{h}{b}}\cdot\frac{k(v)\Omega_2(t)}{\pi}\sqrt{\frac{\xi_1}{c_s\tau}}+O(\xi_1^{3/2})\end{aligned}\right\}, \quad (42)$$

as $\xi_1 \to 0^+$, where $K_I^d(t)$ has been given in eqn (36) and

$$\left.\begin{aligned}\Omega_1(t) &= \frac{1-2\nu}{2(1-\nu)}+\frac{1}{\pi\sqrt{1-\nu}}\Omega_1^{(\mathrm{B})}(t) \\ \Omega_2(t) &= \frac{\sqrt{2(1-2\nu)}}{2(1-\nu)}\sqrt{\frac{h}{a}}\cdot\frac{\omega_0(v)}{\sqrt{t/\tau}}\end{aligned}\right\}.$$

For a transiently propagating mode-I crack in a homogeneous, isotropic, linearly elastic material, Freund and Rosakis (1992) have provided the higher order transient asymptotic representation for the first stress invariant. By using the notation of Liu and Rosakis (1992), for a mode-I crack growing with a constant speed v, we have

$$\left.\begin{aligned}\phi_{,\alpha\alpha}(\xi_1,0^+,t) \;=\; & -\frac{3(1-\alpha_l^2)(1+\alpha_s^2)}{4\mu D(v)}A_0(t)\xi_1^{-1/2} \\ & +\frac{4\alpha_s(1-\alpha_l^2)}{\mu D(v)}A_1(t)+\left\{-\frac{15(1-\alpha_l^2)(1+\alpha_s^2)}{4\mu D(v)}A_2(t)\right. \\ & +\left[\frac{(1-\alpha_l^2)(1+\alpha_s^2)m_l}{D(v)}+\frac{1+\alpha_l^2}{2}\right]D_l^1\{A_0(t)\} \\ & \left.-\frac{2\alpha_s(1-\alpha_l^2)m_s}{D(v)}D_s^1\{A_0(t)\}\right\}\xi_1^{1/2}+O(\xi_1^{3/2})\end{aligned}\right\}, \qquad (43)$$

as $\xi_1 \to 0^+$, where

$$\left.\begin{aligned}D_l^1\{A_0(t)\} &= \frac{3v(1+\alpha_s^2)}{\mu\alpha_l^2c_l^2D(v)}\dot{A}_0(t) \\ D_s^1\{A_0(t)\} &= -\frac{6v\alpha_l}{\mu\alpha_s^2c_s^2D(v)}\dot{A}_0(t)\end{aligned}\right\},$$

and

$$\left.\begin{aligned}m_l &= \frac{1}{2}\left\{\left(1-\alpha_s^2\right)-\frac{2\left(\alpha_l^2-\alpha_s^2\right)}{1-\alpha_l^2}\right\} \\ m_s &= \frac{1}{2}\left(1-\alpha_s^2\right)\end{aligned}\right\}.$$

In eqn (43), $A_0(t)$, $A_1(t)$, and $A_2(t)$ are undetermined functions of time. They cannot be determined by the asymptotic analysis itself. However, for the specific problem at hand, these undetermined functions of time can be obtained by comparing eqns (42) and (43). This comparison yields:

$$\left.\begin{aligned}A_0(t) &= -\frac{\sigma^*\sqrt{c_s\tau}}{\pi}\cdot\frac{\sqrt{2(1-2\nu)}}{2(1-\nu)}\cdot\frac{8k(v)}{3}\sqrt{\frac{b}{a}}\sqrt{\frac{t}{\tau}} \\ A_1(t) &= \sigma^*\cdot\frac{D(v)\Omega_1(t)}{4\alpha_s(1-\alpha_l^2)} \\ A_2(t) &= -\frac{\sigma^*}{\pi\sqrt{c_s\tau}}\cdot\frac{\sqrt{2(1-2\nu)}}{2(1-\nu)}\cdot\frac{k_2(v)}{\sqrt{t/\tau}}\end{aligned}\right\}, \quad t>\tau, \qquad (44)$$

where

$$k_2(v) = \frac{8}{15}\left\{\frac{2(1-\alpha_l^2)(1+\alpha_s^2)m_l}{\alpha_l^2 D(v)} + \frac{8\alpha_l(1-\alpha_s^2)m_s}{\alpha_s(1+\alpha_s^2)D(v)} + \frac{1+\alpha_l^2}{\alpha_l^2} + \omega_0(v)\right\}\frac{hk(v)}{\sqrt{ab}}$$

The variation of the dynamic stress intensity factor $K_I^d(t)$ with time t is plotted in Fig.3 for different crack-tip speeds. In this figure, the

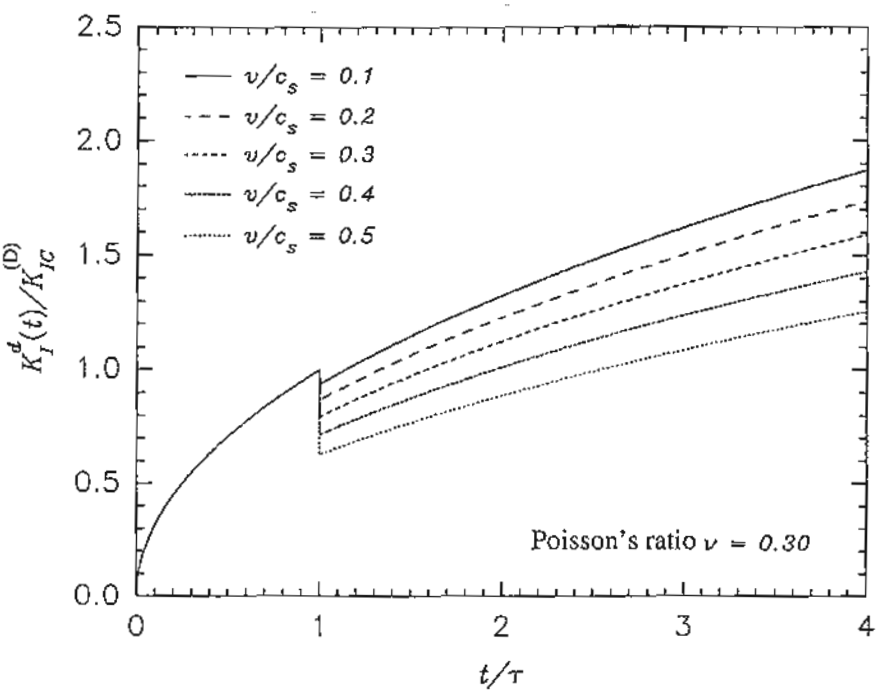

Figure 3: The dynamic stress intensity factor history for the stationary and propagating crack under stress wave loading conditions.

dynamic stress intensity factor is normalized by the critical value of the stress intensity factor at which the stationary crack begins to extend, and the time t is normalized by the delay time τ. These numerical results are obtained by setting the Poisson's ratio $\nu = 0.3$. Before crack initiation, the dynamic stress intensity factor is a monotonic function of time. After crack initiation, the dynamic stress intensity factor monotonically increases with time as well. Although the crack-tip speed is constant, the problem we studied here is characterized as transient, because as the

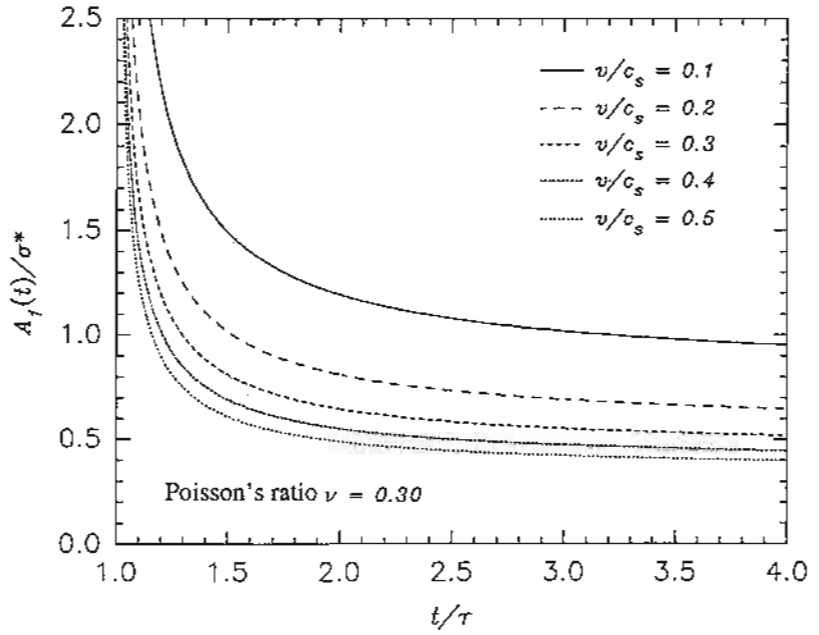

Figure 4: Time history of the coefficient $A_1(t)$ in the higher order transient asymptotic expansion for the moving crack under stress wave loading conditions.

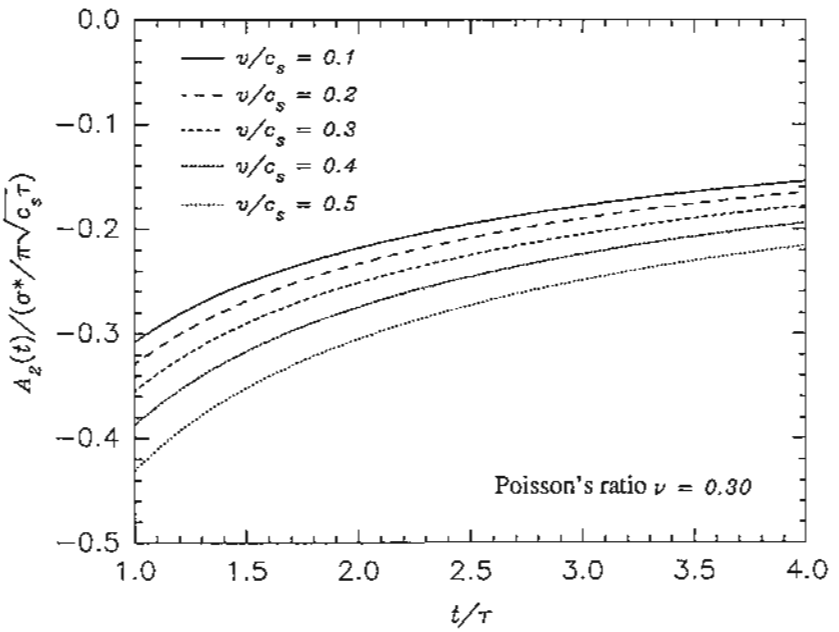

Figure 5: Time history of the coefficient $A_2(t)$ in the higher order transient asymptotic expansion for the moving crack under stress wave loading conditions.

crack starts to grow, the time derivative of the dynamic stress intensity factor is not zero which is contrast with the steady state situation. Notice that in Fig.3, at the time of crack initiation, there is a sudden drop in the value of the dynamic stress intensity factor. This is due to the release of deformation energy by the formation of new crack surfaces associated with crack extension. In addition, the time histories of the coefficients in the higher order transient asymptotic representation of a propagating crack, $A_1(t)$ and $A_2(t)$, are presented in Figs 4 and 5 for different crack-tip speeds. Once again, their time derivatives are not zero due to the transient nature of the problem.

2.4 Study of the normal tractions ahead of the moving crack-tip

In previous sections, we have obtained the complete full field solution for the stresses of the problem described in Section 2. We also obtained the coefficients $A_1(t)$ and $A_2(t)$ of the higher order transient asymptotic expansion. In order to examine whether the full field transient field is representable by either a K_I^d-dominant field or a higher order transient asymptotic field, we will investigate the normal traction ahead of the propagating crack-tip. In other words, we want to investigate the region of dominance of the lowest order and the higher order asymptotic solutions.

By using the analytical results given in Section 2.2 regarding the stresses surrounding the moving crack-tip, the normal traction ahead of the crack-tip, $\sigma_+(\xi_1, t)$ can be calculated from the full field solution. Meanwhile, the normal traction can also be represented by its asymptotic form (up to three terms) as

$$\sigma_+^{(A)}(\xi_1, t) = \frac{K_I^d(t)}{\sqrt{2\pi}}\xi_1^{-1/2} - \frac{15}{4}A_2(t)\xi_1^{1/2} + O(\xi_1), \quad \text{as } \xi_1 \to 0, \qquad (45)$$

where the dynamic stress intensity factor $K_I^d(t)$ and the higher order coefficient $A_2(t)$ have been given in the last section. Here, we have two choices for the asymptotic representation. In regions near the crack-tip where the field is *indeed* K_I^d-dominant, the first term on the right-hand side of eqn (45) will adequately describe the field. Otherwise, higher order terms should be included in order to deal with the lack of K_I^d-dominance.

In Fig.6, the distribution of the normal traction ahead of the moving crack-tip is shown at different instants of normalized time t/τ. One

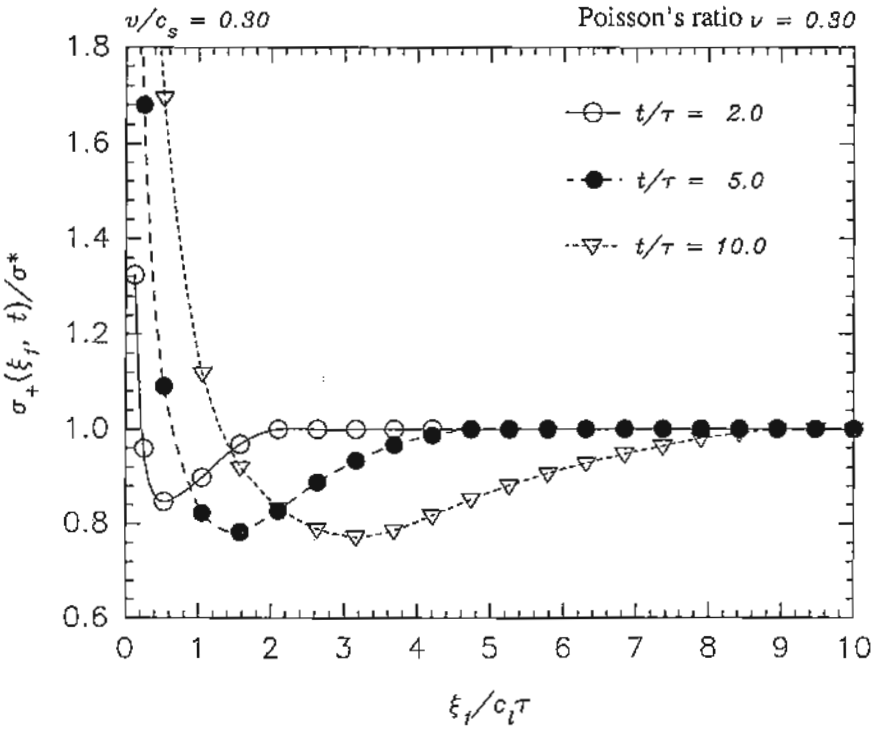

Figure 6: Distribution of normal traction ahead of the moving crack-tip at different instants of time.

should recall here that $t = \tau$ corresponds to the time between the arrival of the stress wave at the crack-tip and initiation of crack growth. This distribution is calculated from the full field analytical solutions presented in previous sections. Here, we have chosen a Poisson's ratio of $\nu = 0.3$ and a crack-tip speed of $v = 0.3c_s$. It should be observed from this figure that at short times after initiation, the singular part of the traction is confined to points very close to the crack-tip and as a result, the region of K_I^d-dominance seems to be initially very small. This issue is investigated in detail later.

Quantitative comparisons of the near tip transient field with either the K_I^d-dominant field or the higher order transient asymptotic field (three term expansion) are given in Figs 7 and 8. In both figures, the normal traction ahead of the moving crack-tip calculated from the analytical result is normalized by its asymptotic representation. The Poisson's ratio is chosen to be 0.3 and the crack-tip speed v is set to be equal to $0.3c_s$. In Fig.7, the variation of the ratio $\sigma_+(\xi_1, t)/\sigma_+^{(A)}(\xi_1, t)$ with respect to

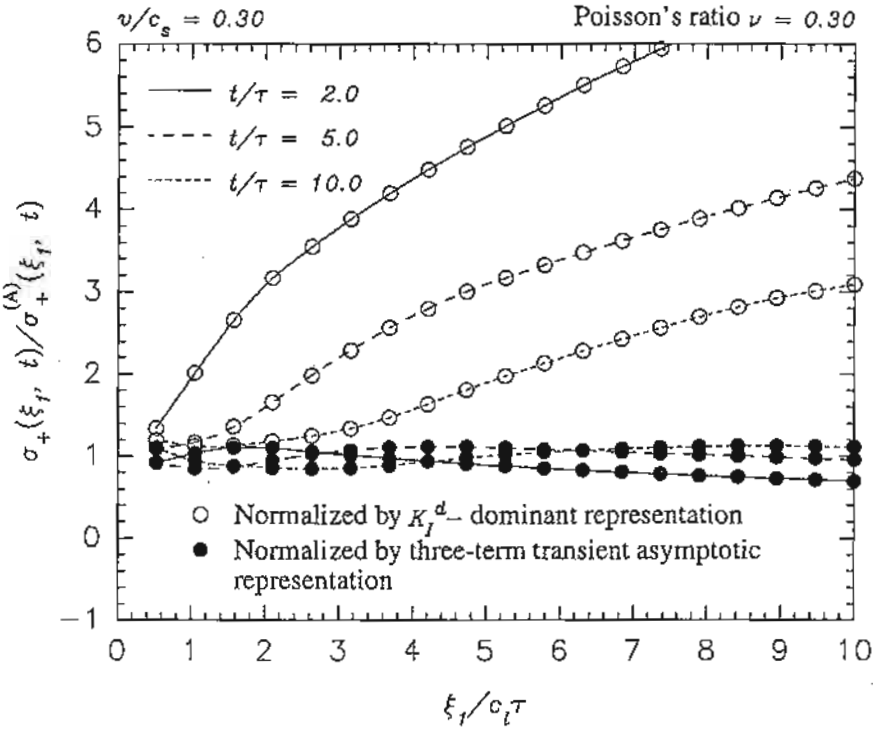

Figure 7: Comparison of the K_I^d-dominant and the higher order transient asymptotic distributions of normal traction ahead of the moving crack-tip at different instant of time after crack initiation.

the nondimensional parameter $\xi_1/c_l\tau$ which represents the distance from the moving crack-tip, is presented. Results for different instants of time after the crack initiation are also presented in this figure. The hollow circles are the value obtained by using the K_I^d-dominant representation, while the solid ones are those obtained by using the higher order transient representation as the asymptotic description (45). To adequately describe the near tip field, the ratio $\sigma_+(\xi_1,t)/\sigma_+^{(A)}(\xi_1,t)$ should be close to 1. However, from Fig.7, we can see that the K_I^d-dominant field deviates substantially from the actual field even when the observation position is at a small distance away from the crack-tip. For the establishment of the fully K_I^d-dominant field near the crack-tip, a rather long time is needed. For example, at the position $\xi_1 = 2c_l\tau$, the time for the K_I^d-dominant field to be established is about $t = 10\tau$. However, the higher order transient asymptotic representation can be seen to approximate the near tip field much closer than the K_I^d-dominant field. Here, even at short times after

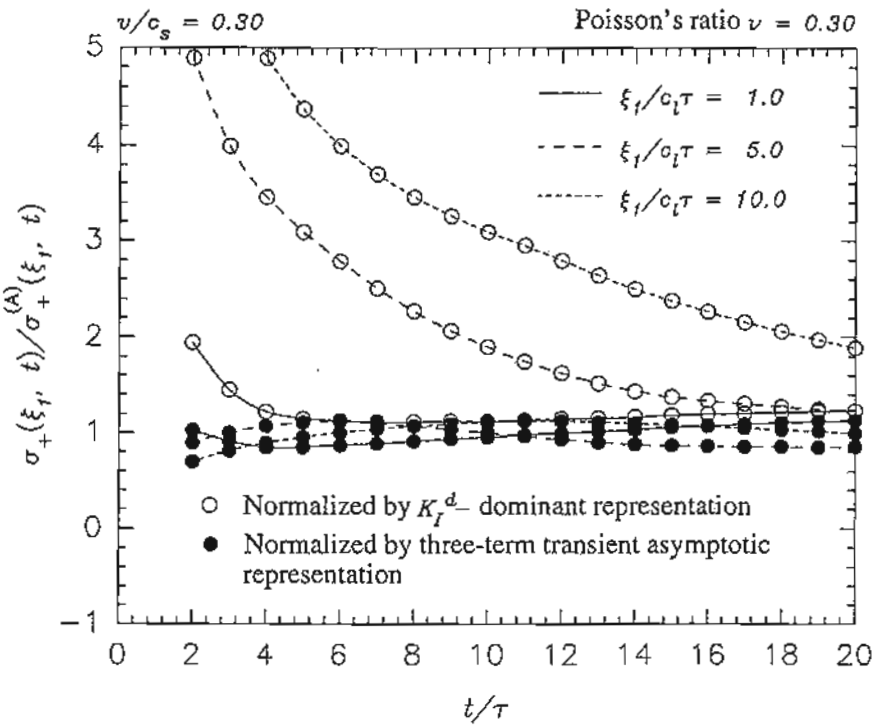

Figure 8: Comparison of the time histories of the K_I^d-dominant and the higher order transient asymptotic representation of normal traction ahead of the moving crack-tip at different distances from the crack-tip.

crack initiation, say $t = 2\tau$, and within a distance $\xi_1 \leq 6c_l\tau$, the result obtained from the higher order transient asymptotic field is about 90% of the value of actual field. Similar observation can be made in Fig.8. Here, the variation of the ratio $\sigma_+(\xi_1, t)/\sigma_+^{(A)}(\xi_1, t)$ is plotted against the nondimensional time t/τ for different positions ahead of the moving crack-tip. In this figure, attention is focused on a moving point which is at a fixed distance relative to the crack-tip. The time required for the K_I^d-dominant field to be established is then calculated. Once again, long times are required for the K_I^d-dominant field to approach the actual field, while at a fixed position relative to the crack-tip the field is well described by the higher order transient representation even at times very close to the crack initiation. Based on these observations, we conclude that conditions of K_I^d-dominance exist either extremely close to the crack-tip or are eventually established at long times after crack initiation. However, the higher order transient asymptotic representation is more successful

in describing the actual field even at times close to the event of crack initiation or at distances relatively far away from the moving crack-tip. Similar observations were also made by Ma and Freund (1986). They considered the problem of a semi-infinite crack subjected to a uniform step pressure on its surface. After a finite delay time, the crack starts to propagate with a constant speed.

2.5 Remarks on the analytical solution

Since Yoffe (1951) mathematically determined the stress field around the tip of a steadily propagating crack with constant length, substantial progress has been made in the areas of theoretical and numerical analysis of dynamic fracture events in brittle materials. The uniqueness of the near tip stress field of a running crack was proved by Freund and Clifton (1974). Their work also established that for a running crack the *near tip* stress state can be characterized by a single parameter – the dynamic stress intensity factor. However, interpretation of the stress field near the edge of a crack in a loaded body in terms of a stress intensity factor must always be based on the assumption that the dimensions of the body and the details of the loading are such that a stress intensity factor controlled (K_I^d-dominant) field does indeed exist and the size of this K_I^d-dominant field is sufficiently small compared to the crack length, distance to the nearest boundary, or any other characteristic dimension of the body. In addition to the limitation noted above concerning overall body dimensions and crack length, the zone of influence of three-dimensional effects around the crack edge should also be small compared to the K_I^d-dominant field, especially when the case of a through thickness crack in a plate is considered. Typically, the plane stress assumption is valid only for points at half of the plate thickness away from the crack edge (Rosakis and Ravi-Chandar, 1986; Yang and Freund, 1985).

If a cracked body is subjected to stress wave loading and the crack growth process is dynamic, there is yet another important factor which complicates the application of the stress intensity factor idea under conditions of plane deformation. This factor is due to the wave character of the mechanical fields in the body during crack growth. Consider, for example, the case studied in the previous sections. This corresponds to a semi-infinite crack in an otherwise unbounded elastic body subjected to stress wave loading conditions. Even though this semi-infinite configuration strictly satisfies all of the size requirements mentioned above,

the application of the K_I^d-dominant field is still limited. Before initiation, when the incoming stress wave hits the crack, the stress wave will diffract around the crack-tip. A cylindrical longitudinal wave and a cylindrical shear wave will be emitted from the crack-tip and will propagate into the body. The assumption of K_I^d-dominance is valid only for points much closer to the crack-tip than the distance of the cylindrical shear wave front from the crack-tip. After crack initiation, the situation becomes even more complicated because stress waves are continuously emitted from the moving crack-tip. This can be seen by observing that the internal stress in the elastic body at a point on the prospective fracture plane will gradually build up as the crack-tip approaches and that this gradually accumulated stress is then suddenly released with the passage of the crack-tip. As a result, the transient fields must radiate out continuously through the region surrounding the propagating crack-tip. This lack of K_I^d-dominance was studied theoretically by Ma and Freund (1986) and was observed experimentally by Krishnaswamy and Rosakis (1991) and Krishnaswamy *et al.* (1992) by using a bifocal caustics arrangement and the optical method of CGS.

By studying the specific problem of a stress wave loaded semi-infinite precrack which eventually extends with a constant speed, we show that the assumption of K_I^d-dominance is inadequate in describing the near tip stress state at short times after crack initiation. For this problem, the transient effect is manifested through the time derivative of the dynamic stress intensity factor even if the crack-tip speed is constant. This study suggests that the use of the higher order transient asymptotic representation provided by Freund and Rosakis (1992), and by Liu and Rosakis (1992) is necessary to represent the actual field near the moving crack-tip. The work described above clearly shows that the coefficients of this expansion depend on the time derivative of the dynamic stress intensity factor. It is further shown that by including this higher order term in the asymptotic expansion, the nature of the near tip stress field is indeed captured. Because of the loss of K_I^d-dominance, even when the body is unbounded and the crack is semi-infinite, this study also suggests that the transient effects should be considered when any attempt is made to interpret experimental measurements performed at finite distances away from the moving crack-tip. In the next section, we will use the results obtained in this section to interpret the experimental observation made by Prakash and Clifton (1992) where crack initiation and growth was studied under extremely high loading rates.

3 Comparison of the theoretical predictions to high loading rate plate impact fracture experiments in AISI 4340 steel

3.1 Introduction

As a material parameter, the fracture toughness can only be obtained through experimental measurements. Meanwhile, the fracture resistance of materials is generally understood to vary with loading rate. Under impact loading conditions, high loading rates are caused at the pre-existing crack-tip. In dynamic fracture experiments, a parameter is defined to characterize the loading rate under which the specimen is loaded, and it is

$$\dot{K}_I = \frac{K_{IC}}{t_C}, \tag{46}$$

where K_{IC} is the mode-I critical stress intensity factor at the instant of crack initiation (fracture toughness) and t_C denotes the time from the beginning of loading to the instant at which fracture initiation occurs. Usually, the crack-tip loading rates range from $\dot{K}_I \sim 1$ MPa$\sqrt{\text{m}} \cdot \text{sec}^{-1}$ for quasi-static loading to as high as $\dot{K}_I \sim 10^8$ MPa$\sqrt{\text{m}} \cdot \text{sec}^{-1}$ for impact loading. Due to the presence of material inertia and strain rate, the material may exhibit totally different behaviors from those under quasi-static loading conditions. To understand the mechanism of crack initiation, propagation, and arrest, various specimen configurations and loading devices have been designed, and extensive research has been carried out for various materials by using different experimental techniques. Using the method of optical caustics, Kalthoff *et al.* (1979) have studied rapid crack propagation and arrest in double-cantilever beam specimen made of Araldite B. Using the same experimental technique and specimen configuration, Rosakis *et al.* (1984) studied crack growth in 4340 steel. Kobayashi and Dally (1980) investigated the crack growth in double cantilever beam 4340 steel specimen but using the method of dynamic photoelasticity. Ravi-Chandar and Knauss (1982) studied the dynamic fracture in Homalite 100 material under stress wave loading. Zehnder and Rosakis (1990) have conducted studies on crack initiation and propagation in 4340 steel using a three point bend configuration impacted by a drop weight hammer.

The interpretation of experimental observations involving dynamic

fracture under stress wave loading has however proven difficult. This is because the specimen configurations commonly used in laboratory testing, cannot be completely modeled by existing mathematical methods, even when the material response is assumed to be linear elastic. The stress waves generated either by the external loading or by radiation from the extending crack-tip, reflect back and forth inside the specimen so that the stress state surrounding the crack-tip is too complicated to be analyzed. Even in cases of specimen configuration such as the one designed by Beinert and Kalthoff (1983), which minimizes dynamic effects caused by wave reflection, direct mathematical analysis is still impossible.

So far, the only geometrical configurations for which it is possible to obtain exact solutions for the elastodynamic fields by solving an initial/boundary value problem, are ones involving infinite straight cracks and unbounded bodies. For the problem of semi-infinite crack loaded by a planar stress wave which after a finite delay time starts to extend with a constant speed, the procedure of getting the complete transient solution has been discussed by Freund (1973 and 1990). The time history of the dynamic stress intensity factor was also obtained and was generalized to include the situation where the crack propagates with a nonuniform speed. In the previous section, we have revisited this problem and obtained the full field analytical solution for the stresses surrounding the stationary and moving crack-tip. In addition, we have also obtained the expressions for the coefficients that appear in a newly developed higher order transient asymptotic representation of the near tip field of a transiently growing crack (Freund and Rosakis, 1992; Liu and Rosakis, 1992). We have shown that this higher order transient representation is able to accurately describe the actual crack-tip field.

Ravichandran and Clifton (1989) have developed a novel experimental configuration which involves loading a half plane crack by a planar tensile pulse. This experimental method is designed to provide comparatively straightforward interpretation of experimental observation within the framework of dynamic fracture mechanics. In this configuration, a disc containing a pre-fatigued edge crack in its mid-plane is impacted by a thin flyer plate of the same material. The resulting compressive pulse propagates through the specimen and reflects from the rear surface as a step, tensile pulse with a duration of about 1μsec. This plane wave loads the crack and causes dynamic initiation and propagation of the crack. Within the duration of loading and the extension of the crack, no unloading waves reach the crack-tip. Therefore, this loading condition corresponds to a semi-infinite crack subjected to a finite duration plane

pulse. By using this experimental technique, one can attain loading rates of approximately $\dot{K}_I \sim 10^8$ MPa$\sqrt{\text{m}} \cdot \text{sec}^{-1}$. This unique configuration allows for the study of dynamic fracture processes which occur when the loading times are in the submicrosecond range.

Prakash and Clifton (1992) studied the process of crack initiation in a hardened AISI 4340 VAR steel by using the high loading rate plate impact experimental procedure described above. The total time period of their experiment was approximately 1μsec. They monitored the motion of the rear surface of the disc at four different points simultaneously during the experiment by using a multiple beam laser interferometer system. An important observation they made in these experiments is the appearance of a clearly marked change in the free surface velocity at all four points at times that correspond to the arrival of waves emanating from the crack-tip during fracture initiation. Meanwhile, they also simulated the dynamic process numerically using a visco-plastic finite difference code. The measured normal velocity of the rear surface of the specimen at a typical monitoring point agrees well with computed scattered fields except for the appearance of a sharp spike in the experimental data of a very short duration. To provide an interpretation for the existence of these spikes, Prakash *et al.* (1992) developed a mathematical model where they assumed that at the moment of initiation, a small, but with finite size, hole suddenly appears at the crack-tip. The stress field associated with this small hole radiates out into the body, and the dominant singularity of this field is $O(r^{-3/2})$ which is stronger than the singularity caused by the sharp crack itself as the crack-tip is approached. In this case, the jump in the particle velocity on the wavefront is infinite, a fact that is consistent with the existence of a spike. However, one should recall that the measurements in their experiments were carried out at points relatively far away from the initial crack-tip. In such points, the information associated with the stronger singularity would die out even faster than the inverse square root term corresponding to the K_I^d-dominant field. This observation has motivated us to seek a second, possible explanation for this phenomenon which lies totally within the realm of classical transient elastodynamics of crack initiation and growth.

In this section, we provide an alternative interpretation to the experimental observations made by Prakash and Clifton (1992). In Section 2 of this chapter, we have obtained the full field analytical solution for stresses surrounding the crack-tip. In addition, the coefficients in the higher order transient asymptotic representation developed by Freund

and Rosakis (1992) and by Liu and Rosakis (1992), have also been calculated. Based on these results, we simulate the experimental observation by using some parameters provided in the experiments. In the next section, the experimental technique and procedure are briefly described. In Section 3.3, the higher order transient asymptotic representation of the particle velocity field is derived by using the result given in Liu and Rosakis (1992). In this asymptotic representation, transient effects including the time derivative of the dynamic stress intensity factor and the crack-tip acceleration are taken into account. In the same section, we use parameters from the experimental measurement, namely, the delay time for crack initiation τ and the amplitude of the incident stress pulse σ^*, to simulate the experimental output. This is done by using the higher order transient representation and by initially assuming constant crack-tip speed. The result shows that the higher order transient representation successfully captures the overall features of the experimental observation, i.e., a finite jump at the time of crack initiation is observed. To predict the experimental observations more accurately, we subsequently relax the restriction of constant crack-tip speed. To do so, in Section 3.4, we first introduce a fracture criterion that relates the dynamic stress intensity factor to the speed of the propagating crack. The fracture criterion is motivated by the experimental measurements made by Zehnder and Rosakis (1990) on the same steel. By solving the crack-tip equation of motion, all time-dependent quantities in the higher order transient asymptotic representation are determined. The simulation of the experimental observation shows that the fully transient asymptotic field can describe the actual field very well. The information regarding the changes of the dynamic stress intensity factor and the crack-tip acceleration associated with crack initiation that are carried out by the term with $r^{1/2}$, seems to be enough to explain the formation of the spikes seen in the experiments.

3.2 Description of plate impact experiments

A very detailed description of the experiment has been provided by Ravichandran and Clifton (1989) and by Prakash and Clifton (1992). The experiment is designed to load a semi-infinite crack by a planar longitudinal tensile wave impinging at normal incidence. The specimen consists of a round disc of 63mm in diameter and 8mm in thickness, which contains a pre-fatigued edge crack that has propagated half way across the diameter. The crack is situated at the mid-plane of the disc.

The specimen is impacted by a plate flyer made of the same material as the specimen. The thickness of the flyer is 3mm. Compressive waves of uniaxial strain are generated by the impact. The wave propagating through the specimen reflects from the rear surface and subjects the crack plane to a step tensile pulse. As the incident tensile pulse hits the crack, part of it is reflected from the crack surface as a compressive wave and part of it is diffracted at the crack-tip. The wave patterns of diffraction and reflection are shown in Fig.9. As we can see from this figure, the

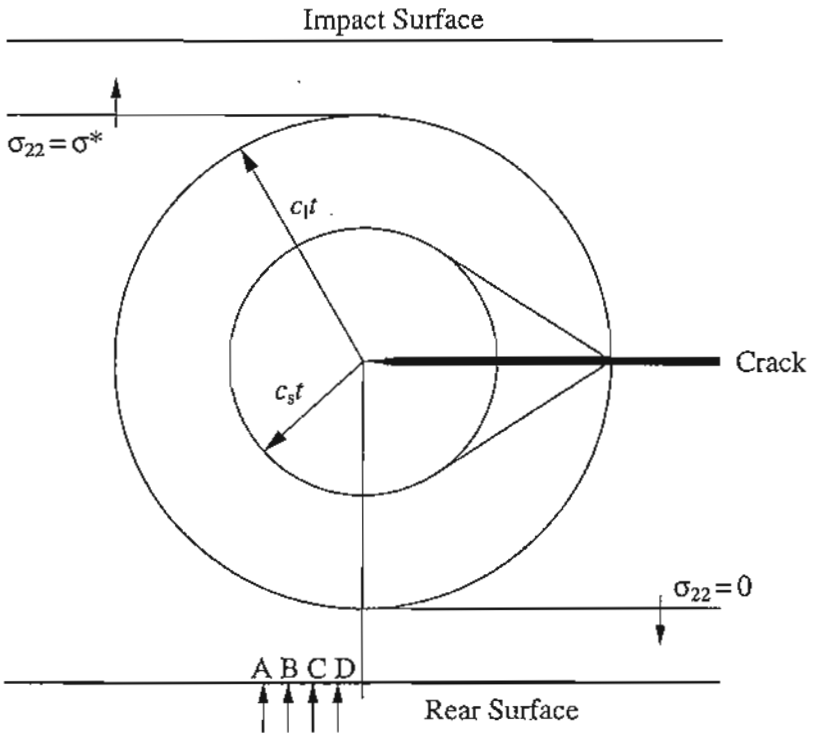

Figure 9: Wavefronts for the diffraction of a planar wave by a semi-infinite crack.

transmitted wave ahead of the crack-tip will be reflected from the front surface of the specimen and the reflected compressive wave will be reflected from the rear surface of the specimen. Before these two waves reach the crack-tip, the stress state near the crack-tip can be modeled as a planar wave diffracted by a semi-infinite crack in an unbounded body.

The material used in the experiments is AISI 4340 VAR steel. This is a high-strength, low-ductility, structural alloy having reduced levels of phosphorus and sulfur to enhance the fracture toughness. Consequently,

the choice of material allows the experimental results to be interpreted within the framework of elastodynamic fracture mechanics. The specimen is cut from a notched cylindrical bar in which a fatigue crack has been grown by subjecting the bar to cyclical bending. In order to produce a homogeneous martinsitic microstructure, special care has been taken in the process of heat treatment of the material.

The motion of four different points on the rear surface of the specimen is monitored by using the interferometric technique. The experimental configuration is shown in Fig.10. A fiberglass projectile which carries the

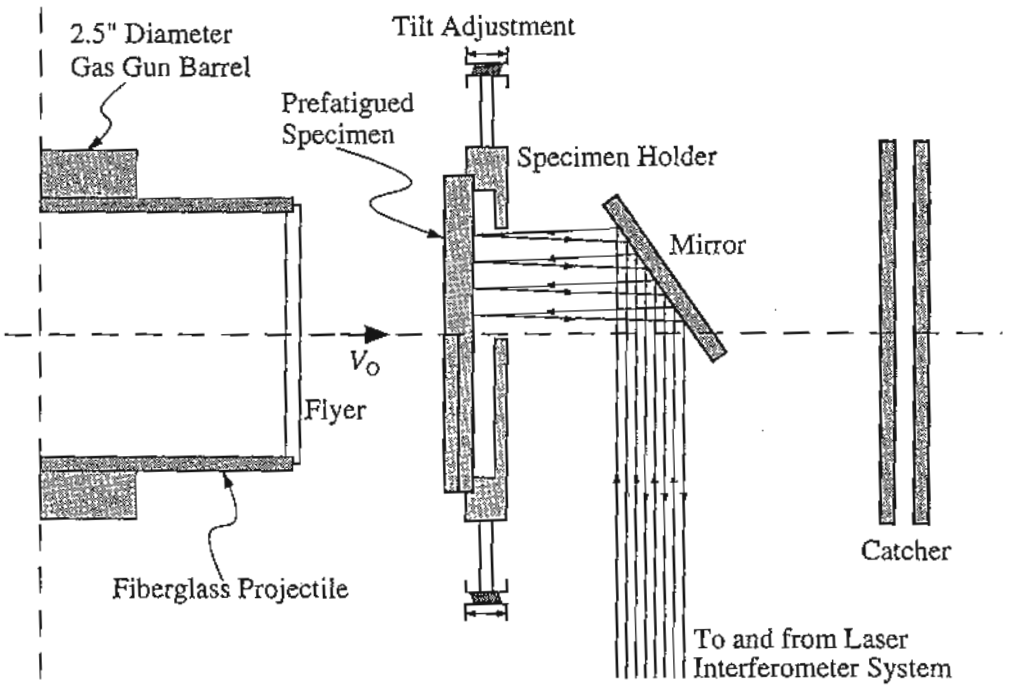

Figure 10: Schematic of the experimental configuration.

flyer plate is accelerated by the nitrogen gas releasing at prescribed pressure and is propelled down the gas gun barrel. The velocity of impact is measured within an accuracy of 1% so that the amplitude of the stress pulse σ^* can be determined fairly accurate. The impact signal triggers the recording system and the motion history of each point monitored on the rear surface of the specimen is obtained. The duration of loading is determined by the thickness of the flyer plate. For this special design of the experimental configuration and the specimen material, the

loading duration is approximately 1μsec. Meanwhile, the design of the experimental configuration ensures that within the duration of loading, no unloading waves reach the crack-tip (see Ravichandran and Clifton, 1989; Prakash and Clifton, 1992).

A typical recording of the experiment obtained by Prakash and Clifton (1992) is shown in Fig.11. This figure shows the particle velocity-time

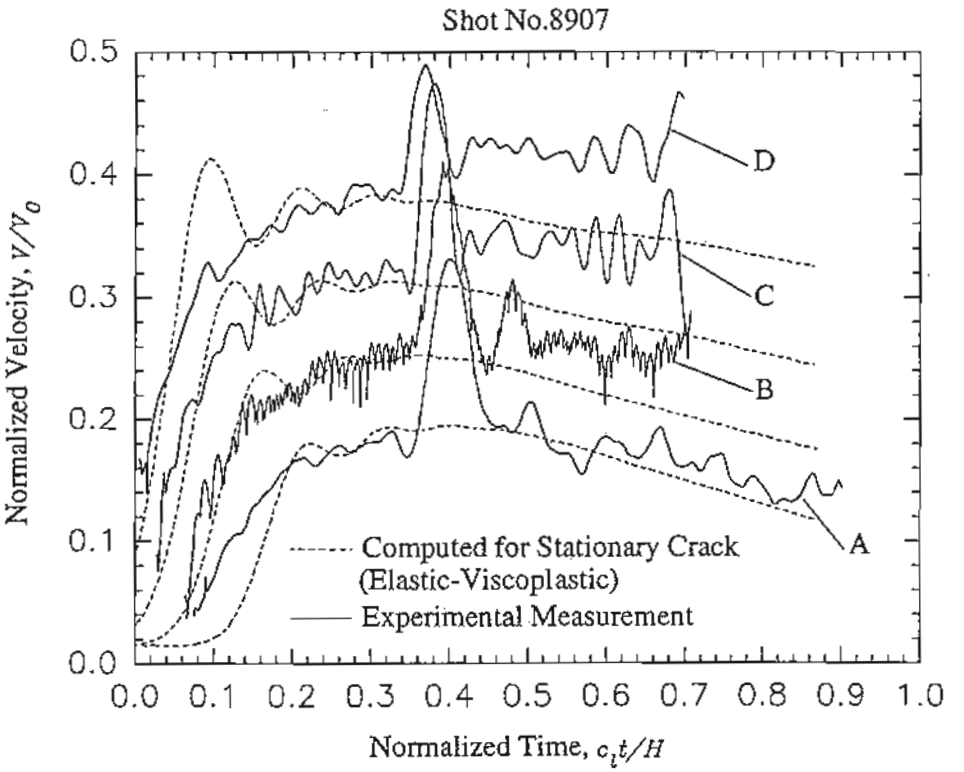

Figure 11: Experimental and numerical predicted (stationary crack) velocity-time profiles at four different monitoring points, from Prakash and Clifton, 1992.

profiles of the rear surface motion at the four monitoring points ahead of the crack-tip. The horizontal axis has been normalized by the characteristic time H/c_l, where c_l is the longitudinal wave speed of the AISI 4340 VAR steel and H is the half thickness of the specimen. The measured particle velocity has also been normalized by the impact velocity V_0 which is 0.0854mm/μsec for this particular experiment. The closest monitoring point is located 0.68mm ahead of the crack-tip. The remaining three

monitoring points are spaced at 0.48mm intervals. In the figure, the solid lines correspond to the recorded velocity-time profiles at those four monitoring points from A to D, which get closer and closer to the crack-tip. The dashed curves correspond to the numerical simulation of the experiment using the elastic-viscoplastic model of the material described in Ravichandran and Clifton (1989), which assumes that the crack remains stationary. Agreement between the computed and experimentally obtained particle velocity histories at the four monitoring points is seen to be very good up to the time which is understood to correspond to the instant of crack initiation. After this time, the experimental and computed velocity-time profiles deviate. An interesting observation from this figure is the appearance of sharp spikes of very short duration at instant corresponding to the crack initiation. As the stress wave emitted due to the crack growth reaches the observation point, the particle velocity increases drastically and then drops very quickly. In the following sections, we will provide an interpretation of these spikes by using the analytical results obtained in Section 2 and the higher order transient asymptotic representation developed by Freund and Rosakis (1992) and by Liu and Rosakis (1992).

3.3 Higher order transient asymptotic representation of the particle velocity field

By using the asymptotic methodology introduced by Freund (1990), and by relaxing the assumptions of K_I^d-dominance and steady state, Freund and Rosakis (1992) have provided a higher order asymptotic expansion for the first stress invariant and have shown that this expansion provides an accurate description of crack-tip fields under fairly severe transient conditions. Rosakis *et al.* (1991) have also obtained all of the components of the higher order asymptotic stress field near the tip of a non-uniformly propagating mode-I crack. For the most general transient situation, i.e., a crack propagates transiently along an arbitrary path, the asymptotic elastodynamic field has been obtained by Liu and Rosakis (1992). In this section, we provide the higher order transient asymptotic representation for the particle velocity field surrounding the moving crack-tip. Based on this representation, we will further offer a possible interpretation for the experimental observations described in the previous section.

By using the notation introduced in Liu and Rosakis (1992), for mode-I deformation, the two components of the higher order transient

asymptotic representation for the particle velocity field surrounding a transiently moving crack-tip are:

$$\left.\begin{aligned}
&\dot{u}_1(\xi_1,\xi_2,t) = -\frac{vK_I^d(t)}{\mu\sqrt{2\pi}}\left\{\frac{1+\alpha_s^2}{D(v)}r_l^{-1/2}\cos\frac{\theta_l}{2} - \frac{2\alpha_l\alpha_s}{D(v)}r_s^{-1/2}\cos\frac{\theta_s}{2}\right\}\\
&-\frac{2v\alpha_s(1-\alpha_s^2)}{\mu D(v)}A_1(t) - v\left\{\left[-\frac{15(1+\alpha_s^2)}{4\mu D(v)}A_2(t) + f_l(t)\right]\cos\frac{\theta_l}{2}\right.\\
&\left.+\left[\frac{1}{8}D_l^1\{A_0(t)\} - \frac{3+\alpha_l^2}{16(1-\alpha_l^2)}B_l(t)\right]\cos\frac{3\theta_l}{2} + \frac{1}{32}B_l(t)\cos\frac{7\theta_l}{2}\right\}r_l^{1/2}\\
&-v\alpha_s\left\{\left[\frac{15\alpha_l}{2\mu D(v)}A_2(t) + g_s(t)\right]\cos\frac{\theta_s}{2}\right.\\
&\left.+\left[\frac{1}{8}D_s^1\{A_0(t)\} + \frac{1-5\alpha_s^2}{16(1-\alpha_s^2)}B_s(t)\right]\cos\frac{3\theta_s}{2} + \frac{1}{32}B_s(t)\cos\frac{7\theta_s}{2}\right\}r_s^{1/2}\\
&+ O(r_{l,s})
\end{aligned}\right\}, \tag{47}$$

and

$$\left.\begin{aligned}
&\dot{u}_2(\xi_1,\xi_2,t) = -\frac{vK_I^d(t)}{\mu\sqrt{2\pi}}\left\{\frac{\alpha_l(1+\alpha_s^2)}{D(v)}r_l^{-1/2}\sin\frac{\theta_l}{2} - \frac{2\alpha_l}{D(v)}r_s^{-1/2}\sin\frac{\theta_s}{2}\right\}\\
&+v\alpha_l\left\{\left[-\frac{15(1+\alpha_s^2)}{4\mu D(v)}A_2(t) + g_l(t)\right]\sin\frac{\theta_l}{2}\right.\\
&\left.-\left[\frac{1}{8}D_l^1\{A_0(t)\} + \frac{1-5\alpha_l^2}{16(1-\alpha_l^2)}B_l(t)\right]\sin\frac{3\theta_l}{2} - \frac{1}{32}B_l(t)\sin\frac{7\theta_l}{2}\right\}r_l^{1/2}\\
&+v\left\{\left[\frac{15\alpha_l}{2\mu D(v)}A_2(t) + f_s(t)\right]\sin\frac{\theta_s}{2}\right.\\
&\left.-\left[\frac{1}{8}D_s^1\{A_0(t)\} - \frac{3+\alpha_s^2}{16(1-\alpha_s^2)}B_s(t)\right]\sin\frac{3\theta_s}{2} - \frac{1}{32}B_s(t)\sin\frac{7\theta_s}{2}\right\}r_s^{1/2}\\
&+ O(r_{l,s})
\end{aligned}\right\}. \tag{48}$$

In expressions (47) and (48), $v(t)$ is the time dependent crack-tip speed, $K_I^d(t)$ is the dynamic stress intensity factor at the moving crack-tip for mode-I deformation, and $A_1(t)$, $A_2(t)$ are unknown coefficients of higher

order terms. Functions $f_{l,s}(t)$ and $g_{l,s}(t)$ are defined by

$$\left.\begin{aligned}
f_l(t) &= \left\{\frac{(1+\alpha_s^2)m_l}{D(v)} + \frac{3+\alpha_l^2}{8(1-\alpha_l^2)}\right\} D_l^1\{A_0(t)\} - \frac{2\alpha_s m_s}{D(v)} D_s^1\{A_0(t)\} \\
&\quad - \frac{1}{2}\left\{\frac{\overset{*}{D}(v)}{D(v)} + \frac{9}{16} - \frac{\alpha_l^2(1+\alpha_l^2)}{8(1-\alpha_l^2)}\right\} B_l(t) + \frac{\alpha_s(1+\alpha_s^2)}{D(v)} B_s(t) \\
f_s(t) &= \left\{\frac{(1+\alpha_s^2)m_s}{D(v)} + \frac{3+\alpha_s^2}{8(1-\alpha_s^2)}\right\} D_s^1\{A_0(t)\} - \frac{2\alpha_l m_l}{D(v)} D_l^1\{A_0(t)\} \\
&\quad - \frac{1}{2}\left\{\frac{\overset{*}{D}(v)}{D(v)} + \frac{9}{16} - \frac{\alpha_s^2(1+\alpha_s^2)}{8(1-\alpha_s^2)}\right\} B_s(t) + \frac{\alpha_l(1+\alpha_s^2)}{D(v)} B_l(t) \\
g_l(t) &= \left\{\frac{(1+\alpha_s^2)m_l}{D(v)} - \frac{1-5\alpha_l^2}{8(1-\alpha_l^2)}\right\} D_l^1\{A_0(t)\} - \frac{2\alpha_s m_s}{D(v)} D_s^1\{A_0(t)\} \\
&\quad - \frac{1}{2}\left\{\frac{\overset{*}{D}(v)}{D(v)} - \frac{5}{16} - \frac{\alpha_l^2(5-3\alpha_l^2)}{8(1-\alpha_l^2)^2}\right\} B_l(t) + \frac{\alpha_s(1+\alpha_s^2)}{D(v)} B_s(t) \\
g_s(t) &= \left\{\frac{(1+\alpha_s^2)m_s}{D(v)} - \frac{1-5\alpha_s^2}{8(1-\alpha_s^2)}\right\} D_s^1\{A_0(t)\} - \frac{2\alpha_l m_l}{D(v)} D_l^1\{A_0(t)\} \\
&\quad - \frac{1}{2}\left\{\frac{\overset{*}{D}(v)}{D(v)} - \frac{5}{16} - \frac{\alpha_s^2(5-3\alpha_s^2)}{8(1-\alpha_s^2)^2}\right\} B_s(t) + \frac{\alpha_l(1+\alpha_s^2)}{D(v)} B_l(t)
\end{aligned}\right\}, \tag{49}$$

where

$$\left.\begin{aligned}
A_0(t) &= -\frac{4}{3\sqrt{2\pi}} K_I^d(t) \\
D_l^1\{A_0(t)\} &= -\frac{4\sqrt{v}}{\sqrt{2\pi}\mu\alpha_l^2 c_l^2} \cdot \frac{\mathrm{d}}{\mathrm{d}t}\left\{\frac{\sqrt{v}(1+\alpha_s)}{D(v)} K_I^d(t)\right\} \\
D_s^1\{A_0(t)\} &= \frac{8\sqrt{v}}{\sqrt{2\pi}\mu\alpha_s^2 c_s^2} \cdot \frac{\mathrm{d}}{\mathrm{d}t}\left\{\frac{\sqrt{v}\alpha_l}{D(v)} K_I^d(t)\right\} \\
B_l(t) &= \frac{2v^2(1+\alpha_s^2)\dot{v}}{\sqrt{2\pi}\mu D(v)\alpha_l^4 c_l^4} K_I^d(t) \\
B_s(t) &= -\frac{4v^2\alpha_l\dot{v}}{\sqrt{2\pi}\mu D(v)\alpha_s^4 c_s^4} K_I^d(t)
\end{aligned}\right\}, \tag{50}$$

and

$$\left.\begin{aligned} D(v) &= 4\alpha_l\alpha_s - (1+\alpha_s^2)^2 \\ \overset{*}{D}(v) &= 4\alpha_l\alpha_s + (1+\alpha_s^2)^2 \\ m_l &= \frac{1}{2}\left\{\left(1-\alpha_s^2\right) - \frac{2\left(\alpha_l^2-\alpha_s^2\right)}{1-\alpha_l^2}\right\} \\ m_s &= \frac{1}{2}\left\{1-\alpha_s^2\right\} \end{aligned}\right\}. \tag{51}$$

$(r_{l,s}, \theta_{l,s})$ are two scaled polar coordinate systems traveling with the crack-tip and are defined by

$$r_{l,s} = \left\{\xi_1^2 + \alpha_{l,s}^2(t)\xi_2^2\right\}^{1/2}, \quad \theta_{l,s} = \tan^{-1}\frac{\alpha_{l,s}(t)\xi_2}{\xi_1},$$

where the functions of time $\alpha_{l,s}(t)$ are defined by

$$\alpha_{l,s}(t) = \left\{1 - \frac{v^2(t)}{c_{l,s}^2}\right\}^{1/2},$$

and c_l, c_s are the longitudinal and shear wave speeds of the elastic solid, respectively. As we can see from eqns (47) and (48), the *first terms* in the asymptotic particle velocity field have the same form as those under the steady state conditions and have $r^{-1/2}$ singularities. However, here the crack-tip velocity takes the instantaneous value at each moment and the dynamic stress intensity factor $K_I^d(t)$ may be an arbitrary function of time. In the component $\dot{u}_1$, the second term (spatially constant term) also takes the form of steady state, but $A_1(t)$ may depend on time explicitly. The third terms, which are proportional to $r^{1/2}$, are totally different from the steady state results for $\dot{u}_1$ and $\dot{u}_2$ not only in their coefficients, but also in their angular distributions. Here, the coefficient $A_2(t)$ may be an explicit function of time. From the definitions, we also see that the differential operators $D_{l,s}^1\{A_0(t)\}$ depend on the instantaneous values of the crack-tip speed and the dynamic stress intensity factor, as well as their time derivatives. Meanwhile, $B_{l,s}(t)$ not only depend on the instantaneous values of the crack-tip speed and the dynamic stress intensity factor, but also depend linearly on the crack-tip acceleration. In addition, the dynamic stress intensity factor $K_I^d(t)$ and the higher order coefficients $A_1(t)$ and $A_2(t)$ cannot be determined by the asymptotic analysis itself. They can only be determined by the specific boundary and initial conditions of the problem. If the crack-tip speed $v(t)$ is constant, i.e., if $\dot{v}(t) = 0$, then $B_{l,s}(t) = 0$, and $D_{l,s}^1\{A_0(t)\}$ will linearly

depend on the time derivative of the dynamic stress intensity factor. Under such circumstance, expressions (47) and (48) correspond to transient crack growth with constant velocity and varying stress intensity factor. This is still a transient problem. The problem we solved in Section 2 belongs to this category. Furthermore, if the time derivative of the dynamic stress intensity factor is also zero, then $D^1_{l,s}\{A_0(t)\} = 0$ as well. In this case, the higher order steady state expansion is obtained. However, the coefficients A_1 and A_2 are now time independent.

For the problem at hand, we have obtained the full field analytical solution for the elastodynamic field surrounding the crack-tip in Section 2. Also, we have obtained the coefficients of the higher order terms $A_1(t)$ and $A_2(t)$ for this problem. Therefore, for the case of constant crack-tip velocity but varying dynamic stress intensity factor, we can use expressions (47) and (48), with $B_{l,s}(t) = 0$ for this case, to predict the particle velocity at any position and at any moment. To simulate the observations given in Fig.11, we only need expression (48). However, since the measurement is carried out at the traction free surface of the specimen and eqn (48) is for a point inside unbounded body (traction free condition is not met), the value of the particle velocity $\dot{u}_2$ obtained from eqn (48) has to be multiplied by a factor of two to provide a proper comparison between the analytical and the experimental results. For the particular test (shot No.8907, Prakash and Clifton, 1992), the following parameters obtained from the experiment have been used in the simulation: Impact velocity $V_0 = 0.0854\text{mm}/\mu\text{sec}$, Amplitude of the incident stress pulse $\sigma^* = 1941\text{MPa}$, Delay time $\tau = 0.1905\mu\text{sec}$, Material mass density $\rho = 7600\text{Kg} \cdot \text{m}^{-3}$, Poisson's ratio $\nu = 0.3$, Longitudinal wave speed $c_l = 5.983\text{mm}/\mu\text{sec}$, and Shear wave speed $c_s = 3.124\text{mm}/\mu\text{sec}$.

By using the parameters given above, Fig.12 shows analytical predictions in which we have used the higher order asymptotic representation for the transiently propagating crack with constant speed, to simulate the particle velocity at monitoring point D. In Fig.12, the circles represent the experimental data while the various lines stand for the simulated values. It should be pointed out that in Fig.12, before crack initiation, the simulated particle velocity is calculated from the full field analytical solution obtained in Section 2, while after crack initiation, expression (48) is used. It can be seen that before crack initiation, the particle velocity calculated by using the analytical solution, agrees well with the measurements. At the very beginning, however, deviation exists between the theoretical prediction and the experimental measurement. This is due to the fact that the specimen is preloaded by a compressive pulse

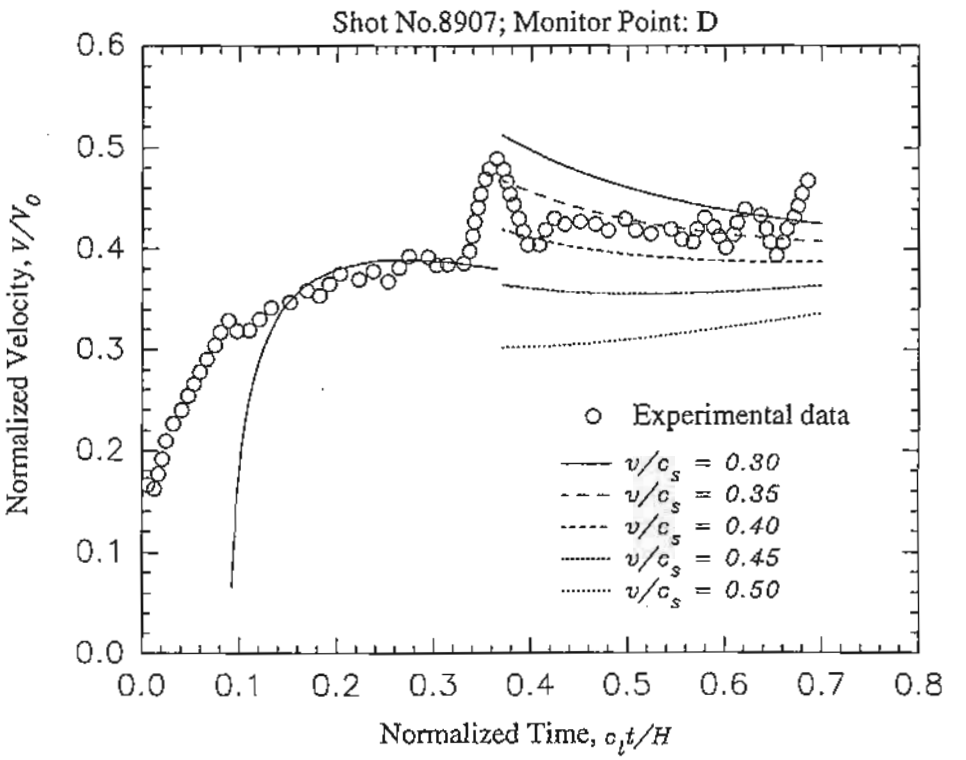

Figure 12: Analytical simulation of the experimental measurement at monitoring point D by Prakash and Clifton (1992), shot No.8907. Before crack initiation, full field expression for the particle velocity is used. After crack initiation, three-term transient asymptotic representation given in eqn.(48) with constant crack-tip speed has been used.

resulting from the initial impact while the mathematical model assumes that the body is loaded directly by a tensile stress pulse. After crack initiation, the velocity-time profile at point D is simulated by the three-term transient asymptotic representation given in eqn (48). Here, $B_{l,s}(t) = 0$, $K_I^d(t)$ and $A_2(t)$ have been given in Section 2 (see eqns (36) and (44) in Section 2). One can see from this figure that by including the transient effect (through the time derivative of the dynamic stress intensity factor $K_I^d(t)$), we are able to capture the most important feature in the experimental observations for a particular choice of crack-tip velocity, i.e., $v \sim 0.33c_s$. At the instant of crack initiation, the particle velocity at the monitoring point does not transit smoothly from the value corresponding to the stationary crack to the value corresponding to the extending crack.

This velocity has a jump at the moment associated with crack initiation and this jump depends on the magnitude of the speed of crack growth.

At this point, some qualitative observations can be made from Fig.12. At the instant of crack initiation, the crack first jumps from stationary to a velocity about $0.3c_s$ after that the crack-tip speed increases quickly and approaches the value of $0.4c_s$. After crack initiation, the crack-tip speed oscillates about the level of $0.35c_s$. It seems that because of the applied stress pulse, deformation energy is accumulated at the tip of the original semi-infinite stationary crack, and if the material is of limited strength, the crack will start to grow and the deformation energy will be released. Part of this released energy is consumed to form new crack surface, another part becomes the kinematic energy of the crack-tip. However, this process is not steady. The extending crack continuously increases its speed to approach a "steady" state, i.e., the crack-tip speed approaches a constant value. Therefore, the formation of the spikes in the experimental observations is attributed to the process of crack initiation and then approaching the steady speed in a very short period of time. This description is only a qualitative speculation and does not provide a complete picture about the dynamic crack initiation and transient crack growth since we have assumed that the crack-tip velocity is constant when we simulate the experimental observation in Fig.12, while change of velocity has been involved in this process. Notice that in the higher order transient asymptotic representation of the field of particle velocity, eqns (47) and (48), the crack-tip acceleration plays a prominent role. Therefore, if we can provide more accurate information regarding the crack-tip speed during the extension, the picture of the transient crack growth will become more complete. However, unlike the fracture experiments based on optical caustics and CGS, the plate impact experimental technique cannot provide an independent crack-tip velocity history. For this reason, in the next section, we will introduce a criterion regarding dynamic crack growth first, and then we can predict the histories of the crack-tip speed by solving the crack-tip equation of motion. After that, we will simulate the experimental observation again by including all of the transient effects (i.e., terms involving both $\dot{K}_I^d(t)$ and $\dot{v}(t)$).

3.4 Crack-tip equation of motion

If the history of the crack-tip motion is specified, then the surrounding mechanical fields in an elastic body can be obtained in principle within

the context of linear elastic continuum mechanics, as long as the configuration of the body and the details of the loading are also specified. However, since the motion of crack-tip is totally controlled by the deformation state inside the surrounding material, the motion of the crack-tip should not be specified a priori. Due to the fact that the constitutive equation for the material does not include the possibility of material separation, we need a mathematical statement of a crack growth criterion to be added into the governing equations. Such criterion must be stated as a physical postulate on material behavior and at the same level as the kinematical theorems governing deformation, momentum balance principles, as well as the constitutive relation describing material response. The most common form for such a criterion is the requirement that the crack must grow in such a way that some parameter defined as part of the crack-tip field maintains a value that is specific to the material. This value, representing the resistance of the material to the advance of the crack, is called the fracture toughness of the material, and it can be determined through experimental measurements only.

During the process of crack growth, if the small scale yielding condition prevails, a possible fracture criterion stipulates

$$K_I^d(t) = K_{IC}^d, \tag{52}$$

where the left-hand side is the dynamic stress intensity factor (in principle entirely determined through an analysis of a boundary/initial value problem) and the right-hand side represents a material quantity called the *dynamic fracture toughness* which can only be determined through experiments. The dynamic stress intensity factor $K_I^d(t)$ is known to be a function of crack length $a(t)$, crack-tip speed $v(t)$, and some generalized measure of the applied load $P(t)$. It has also been suggested that the dynamic fracture toughness must be dependent on crack-tip velocity (Freund, 1990; Rosakis *et al.*, 1984; Zehnder and Rosakis, 1990). Thus the fracture criterion as given in (52) becomes

$$K_I^d\left(a(t), v(t), P(t), t\right) = K_{IC}^d\left(v(t), \cdots\right). \tag{53}$$

Equation (53) is an evolution equation for crack growth, i.e., a crack-tip equation of motion, since it represents a nonlinear, first order differential equation for the crack length $a(t)$.

For the specific problem at hand, the dynamic stress intensity factor for the propagating crack is given by

$$K_I^d(t) = k(v) K_{IC}^{(\mathrm{D})} \sqrt{\frac{t}{\tau}}, \tag{54}$$

where $K_{IC}^{(D)}$ is the value of the dynamic stress intensity factor at the instant of crack initiation (dynamic initiation toughness) and τ is the delay time between the instant of stress wave arrival at the crack and the onset of crack extension (see Section 2.1). $k(v)$ is a universal function of the crack-tip speed v, such that $k(v) = 1$ at $v = 0$ and $k(v) = 0$ at $v = c_R$, where c_R is the Rayleigh wave speed of the material. As for the dynamic fracture toughness, one usually assumes that it is only dependent on the crack-tip velocity and on material characteristics. We can thus express K_{IC}^{d} as

$$K_{IC}^{d}(v) = K_{IC}^{ss} f(v), \tag{55}$$

where K_{IC}^{ss} is the steady state quasi-static crack growth fracture toughness for the material (asymptotic value of the small scale yielding, quasi-static resistence curve). $f(v)$ is a function of crack-tip speed such that $f(v) = 1$ at $v = 0$. As $v \to 0$, $K_{IC}^{d}(v) \to K_{IC}^{ss}$. The relation between the dynamic initiation toughness $K_{IC}^{(D)}$ and K_{IC}^{ss} that appear in eqns (54) and (55) is supposed to be

$$K_{IC}^{(D)} = \alpha K_{IC}^{ss}, \tag{56}$$

where $\alpha \geq 1$. Since K_{IC}^{ss} corresponds to the quasi-static conditions, it represents the situation where the loading rate is close to zero. Here, several effects have been included into the number α. First, it has been observed that the critical value of the dynamic stress intensity factor at crack initiation increases as the loading rate increases. Secondly, in the laboratory situations, the crack-tip cannot be mathematically sharp, and the bluntness of the crack-tip will also increase the critical value for initiation. Even for high strength materials like AISI 4340 steel, some initial plasticity is expected to blunt the fatigue precrack. As a result, the number α is assigned to accommodate the effects of loading rate and initial crack-tip bluntness.

By using relations (54), (55), and (56), the crack-tip equation of motion (53) becomes

$$\alpha k(v) \sqrt{\frac{t}{\tau}} = f(v). \tag{57}$$

The form of the universal function $k(v)$ can be simplified as (Freund, 1990)

$$k(v) = \frac{1 - v/c_R}{\sqrt{1 - v/c_l}}. \tag{58}$$

Also for the purpose of present study and from previous experimental observations regarding the relation between the dynamic fracture tough-

ness and the crack-tip speed, we choose the form of the function $f(v)$ as

$$f(v) = \frac{1 + \frac{1}{M}\tan\left(\frac{\pi}{2}\cdot\frac{v}{v_m}\right)}{\sqrt{1 - v/c_l}}, \tag{59}$$

where M and v_m are two material constants. Notice that $f(v) \to 1$ as $v \to 0$ and $f(v) \to \infty$ as $v \to v_m$, so that v_m represents a "terminal speed" that a crack can achieve in this particular solid. In most of the dynamic fracture experimental measurements, the terminal speed of a mode-I crack in the homogeneous material is about $0.3 \sim 0.5c_R$. To determine the constants M and v_m for the material AISI 4340 VAR steel used in the experiments, we compare the curves given by eqn (59) to the experimental measurements obtained by Rosakis *et al.* (1984) and by Zehnder and Rosakis (1990). These experimental measurements are shown here in Fig.13. In this figure, the circles represent the value obtained from the experiments, and the various lines are obtained from (59) for different value of M. From this figure, we can see that $v_m \sim 0.34c_s$. In the same figure, it seems that $M = 10$ is best fitting for the experimental values. However, one should notice that the material that the experiment used is 4340 steel (see Rosakis *et al.*, 1984; Zehnder and Rosakis, 1990) which is slightly different from the material used in Prakash and Clifton (1992). The heat treatment processes are also different for these two materials. As a result, the material used by Prakash and Clifton (1992) is more brittle than the material used in Zehnder and Rosakis (1990). Another reason for this conclusion is that the loading rates in the experiments by Prakash and Clifton (1992) are much higher than the rate in Zehnder and Rosakis (1990). Under high strain rate, material will also become more brittle. Previous experiments have shown that the more brittle the material is, the more abrupt the $K_I^d - v$ curve becomes. This suggests that larger value of M should be used to simulate the experimental observations in Prakash and Clifton (1992).

By substituting the expressions for $k(v)$ and $f(v)$ into the crack-tip equation of motion (57), we get

$$1 + \frac{1}{M}\tan\left(\frac{\pi}{2}\cdot\frac{v}{v_m}\right) - \alpha\left(1 - \frac{v}{c_R}\right)\sqrt{\frac{t}{\tau}} = 0, \tag{60}$$

from which the time history $v(t)$ of the crack-tip speed can be obtained. Once the crack-tip speed history is determined, the crack-tip acceleration can also be obtained by differentiating the crack-tip speed profile. From

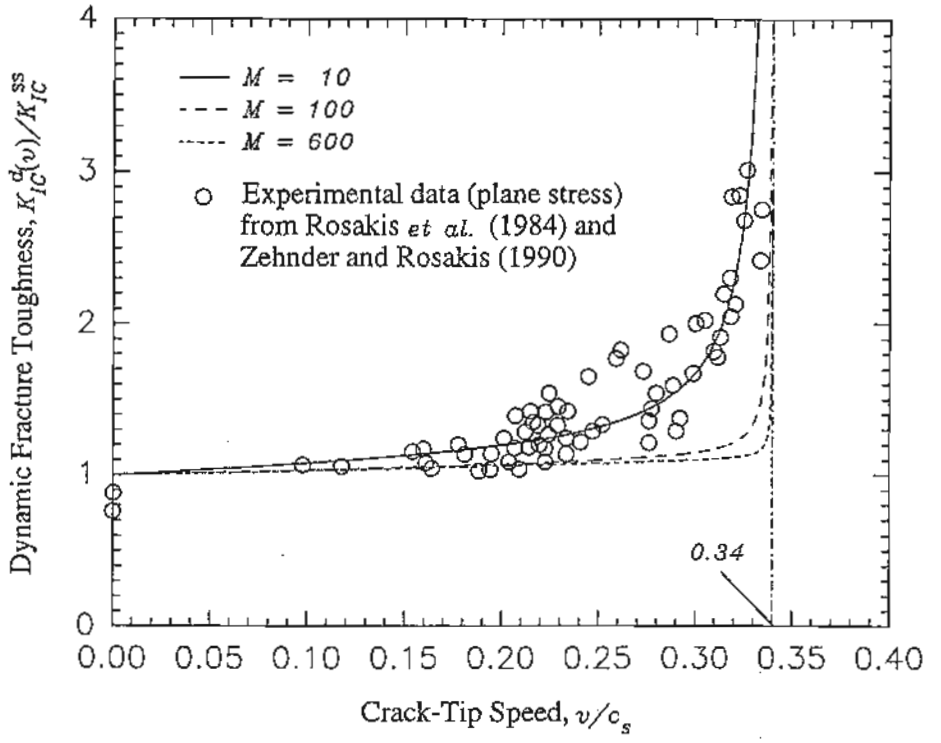

Figure 13: Comparison of the relationship between the dynamic fracture toughness and the crack-tip speed. Different lines represent the prediction using eqn (59) and circles are the experimental results obtained by Rosakis *et al.* (1984) and Zehnder and Rosakis (1990).

eqn (60), we can express the crack-tip acceleration in terms of crack-tip velocity and time t as:

$$\dot{v}(t) = -\frac{\alpha c_R}{2\tau} \cdot \frac{g(v)}{\sqrt{t/\tau}}, \tag{61}$$

where

$$g(v) = \frac{\left\{1 + \left(\frac{\pi}{2} \cdot \frac{v}{v_m}\right)^2\right\}\left(1 - \frac{v}{c_R}\right)^2}{\frac{\pi}{2M} \cdot \frac{c_R}{v_m}\left(1 - \frac{v}{c_R}\right) + \left\{1 + \frac{1}{M}\tan\left(\frac{\pi}{2} \cdot \frac{v}{v_m}\right)\right\}\left\{1 + \left(\frac{\pi}{2} \cdot \frac{v}{v_m}\right)^2\right\}}.$$

Freund (1973) has shown that for an unbounded body under time-independent loading conditions, the dynamic stress intensity factor at

the running crack-tip can be expressed as a universal function of instantaneous crack-tip speed times the equilibrium stress intensity factor for the given applied loading and the instantaneous amount of crack growth. Therefore, for the problem we considered in Section 2, even when the crack propagates with nonuniform velocity, the dynamic stress intensity factor $K_I^d(t)$ is still given by eqn (54), where the velocity v takes the instantaneous value at each instant of time. As a result, the time derivative of the dynamic stress intensity factor under this circumstance will be expressed in terms of the crack-tip speed, acceleration, and the time t as:

$$\dot{K}_I^d(t) = K_I^d(t)\left\{\frac{1}{2t} + \frac{k'(v)}{k(v)}\dot{v}(t)\right\}. \tag{62}$$

By applying the crack growth criterion (53), we have been able to determine the time histories of crack-tip speed, crack-tip acceleration, and the time derivative of the dynamic stress intensity factor. Consequently, the quantities that appear in the higher order transient asymptotic representation of the particle velocity field surrounding the moving crack-tip, i.e., $D^1_{l,s}\{A_0(t)\}$ and $B_{l,s}(t)$ in eqn (50), can be determined as well. However, the explicit expression for the higher order coefficient $A_2(t)$ is obtained under the condition that the crack propagates with a constant velocity (see Section 2). Nevertheless, if we expand the field for the stationary crack subjected to stress pulse (superposition of problems A and B in Section 2) to the third term and compare this term to our expression for $A_2(t)$, we found that $A_2(t)$ has the same property as the dynamic stress intensity factor, i.e., $A_2(t)$ can be expressed as a function of instantaneous crack-tip speed times the equilibrium value of the third term for the given applied loading and the instantaneous amount of crack growth. Based on this observation, we conclude that for a crack propagating with a nonuniform speed, the coefficient of higher order term, $A_2(t)$, has the same form as that for constant velocity except that the crack-tip speed takes the instantaneous value at each instant of time.

The initiation and propagation of a semi-infinite crack subjected to the stress wave loading conditions can be described by Fig.14. In Fig.14, the solid line represents the relation between the dynamic fracture toughness K_{IC}^d and the crack-tip propagating speed $v(t)$. The intersection of this curve to the vertical axis is the value of the critical stress intensity factor of crack initiation under quasi-static conditions, i.e., K_{IC}^{ss}. Also, this curve asymptotically approaches the vertical line denoting the terminal speed of the crack-tip in this material. In the same figure, the

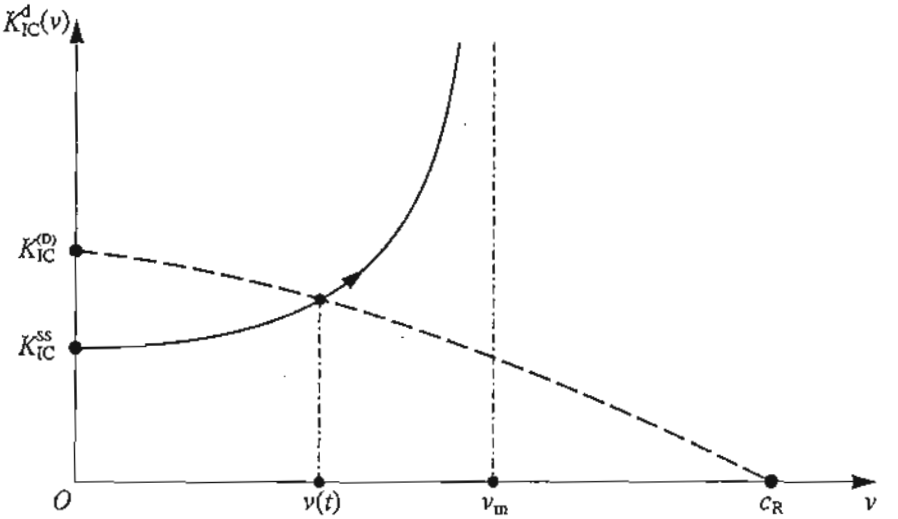

Figure 14: Schematic description of dynamic crack initiation and propagation.

dashed line gives the relationship between the dynamic stress intensity factor $K_I^d(t)$ at the moving crack-tip and the crack-tip speed $v(t)$. The point corresponding to $v = 0$ provides the value of the dynamic stress intensity factor at the stationary crack-tip under stress wave loading. As $v = c_R$, the dynamic stress intensity factor of the moving crack will be zero. At the time $t = \tau$, the initial crack-tip speed and the new value of the dynamic stress intensity factor just after initiation are determined by the intersection point of the solid and dashed lines. As we can see from this geometrical construction, the dynamic stress intensity factor suffers a drop relative to its value immediately before initiation. For this particular loading condition and specimen configuration, the initial crack-tip speed and the drop of the dynamic stress intensity factor are completely determined by the shape of the solid line. In other words, they are determined by the material property described by the crack growth criterion. After crack initiation, since $K_I^d(t)$ is an increasing function of time t, the intersection point will move upward along the crack growth criterion curve. The crack-tip speed will increase as well and finally approach the terminal speed. In Fig.15, the profiles of the crack-tip speed and crack-tip acceleration are plotted. Here, we have chosen $\alpha = 2.0$ and $M = 600$ to simulate a brittle material experiencing high strain rate, and as the

result of Zehnder and Rosakis (1990) suggested, we have also chosen that the terminal speed $v_m = 0.34c_s$.

By using the crack-tip velocity and acceleration histories given in Fig.15 which results from imposing the crack growth criterion depicted in Fig.13, and by using the expressions for $A_2(t)$ obtained in Section 2, we simulate the particle velocity at the monitoring point D again for the experiment presented in Fig.11. This simulation is compared to the experimental results in Fig.16. In this figure, we can see that the theoretical prediction is much closer to the experimental measurement than the theoretical prediction obtained under the assumption of constant crack-tip speed. By imposing the crack growth criterion, the crack-tip first jumps to a relatively low initiation velocity and then quickly approaches its terminal speed. As a result, the particle velocity at the observation point D also jumps to a high value at the moment of crack initiation at first, and then quickly decreases to the average value of the particle velocity measured from the experiment at that point. Notice that even though the theoretical prediction by our current higher order transient asymptotic analysis has captured the essential feature of the experimental observation, the decay of the particle velocity obtained from calculation is not as fast as the experimental result. The reason for this difference is probably due to the fact that the measuring point is relatively far away from the crack-tip, therefore even higher order terms in the asymptotic expansion need to be used.

In the theoretical simulations in the present and the previous sections, we choose to compare the theoretical prediction and the experimental observation from point D only. For other points, like points A, B, and C in Fig.11, the results from theoretical calculation and experimental measurements deviate progressively as the distance from point D is increased. In particular, the further the horizontal distance away from the crack-tip becomes, the larger is the deviation between the theoretical prediction and the experimental measurement. The explanation for this deviation is that when the stress wave diffracts at the stationary crack-tip, or emanates from the moving crack-tip, cylindrical waves radiate from the crack-tip and propagate towards the boundaries of the specimen. As these waves reach the boundary, various kinds of waves are generated from the reflection of the incident wave. If the incident cylindrical wave is longitudinal or transverse, both longitudinal and shear type of reflection waves are generated depending on the incident angle. At the same time, surface waves are generated as well. So the effects of these reflection waves influence the experimental measurements. However, in

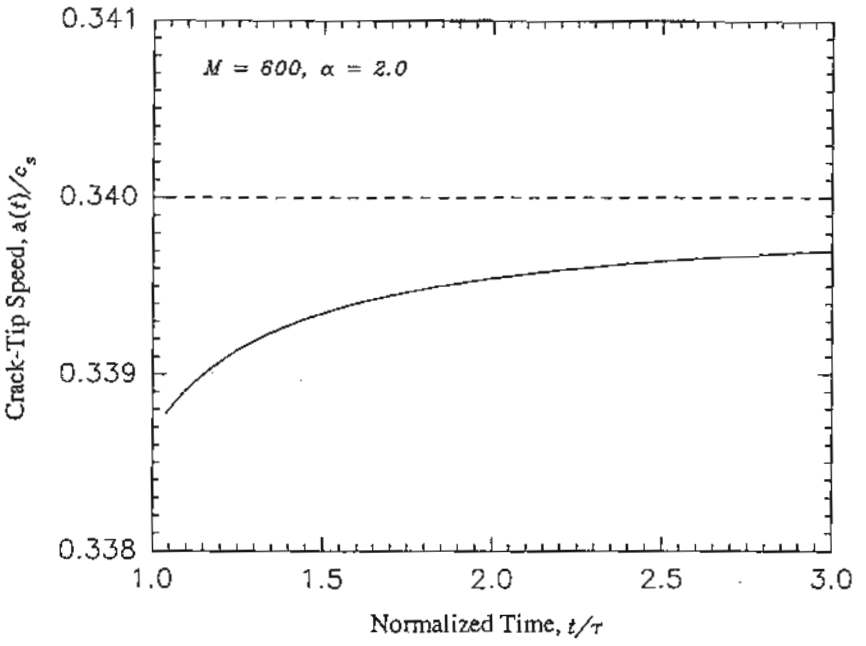

(a)

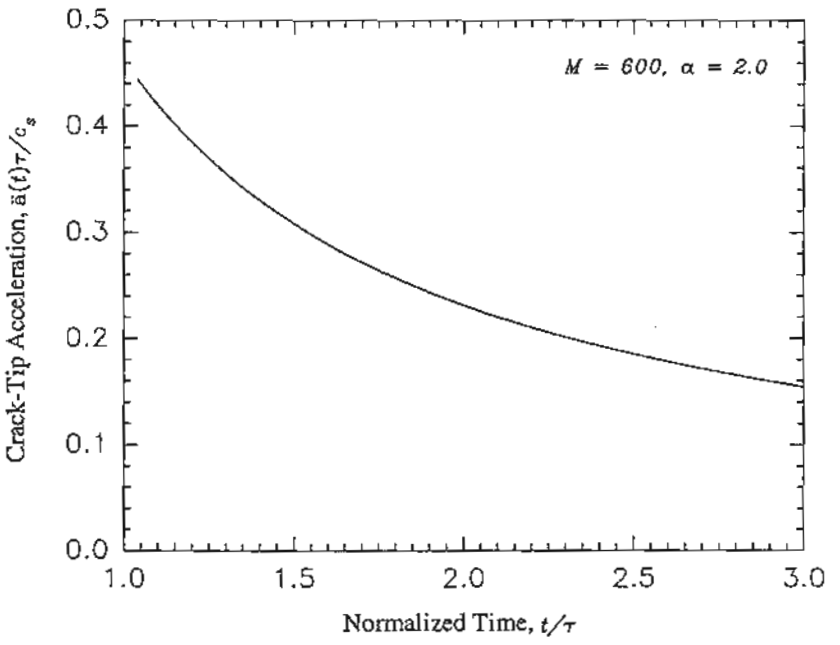

(b)

Figure 15: Time histories of the crack-tip speed (a), and crack-tip acceleration (b), where $\alpha = 2.0$ and $M = 600$ have been chosen.

our mathematical model, the specimen is considered to be unbounded and the theoretical prediction cannot include the free boundary reflection effects. The only point that an accurate simulation can be expected from the theoretical model, is the point just below the crack-tip on the boundary (see Fig.9). At this point, the reflection effect can be accounted for, by multiplying the theoretical value by a factor of two. Unfortunately, there is no further experimental data from such points available for our simulation. As a result, a complete numerical simulation of the experiment is necessary. In such a simulation, the data obtained from points just below the crack-tip can be compared with our theoretical predictions.

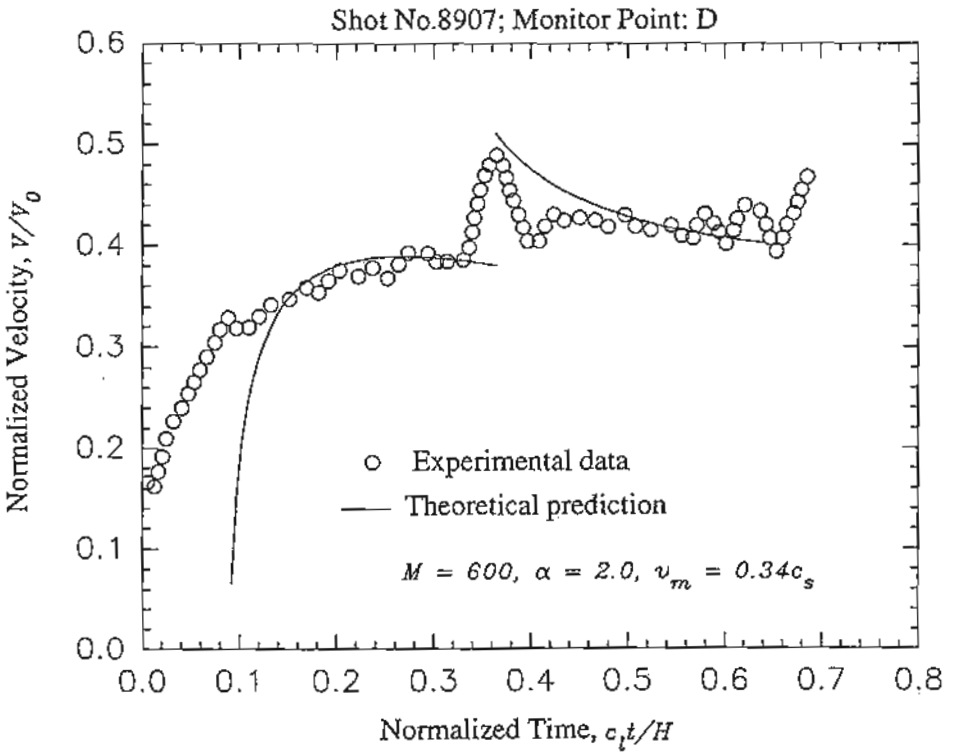

Figure 16: Analytical simulation of the experimental measurement at monitoring point D by Prakash and Clifton (1992), shot No.8907. Before crack initiation, full field expression for the particle velocity is used. After crack initiation, three-term fully transient asymptotic representation given in eqn (48) has been used.

3.5 Discussion and conclusions

The experimental observations made by Prakash and Clifton (1992) are reinterpreted on the basis of the newly developed higher order transient asymptotic analysis by Freund and Rosakis (1992) and by Liu and Rosakis (1992). In this transient asymptotic representation, the leading term in the expansion of the local stress field is the familiar stress intensity factor distribution, that is, it is square root singular in the radial distance from the moving crack-tip and its coefficient is proportional to the instantaneous value of the dynamic stress intensity factor, $K_I^d(t)$. The higher order terms, on the other hand, take into account the recent past history of the stress intensity factor and crack motion. Therefore, the transient nature of the local field is reflected in these higher order terms. It should be noted that from the view point of asymptotic expansion, the coefficient of each term of the asymptotic expansion carries different information about the deformation field. The coefficient of the first term, $K_I^d(t)$, purely represents the intensity or the amplitude of the local stress and deformation fields, and this coefficient depends on the overall specimen configuration and loading condition. The coefficient of the second term, $A_1(t)$, also possesses these properties. Inside the coefficients of the higher order terms, however, more information will be present. One part of the information, like $A_2(t)$, etc. still relates to the overall specimen configuration and loading condition. The other part will relate to the crack-tip acceleration, time derivatives of the coefficients of the lower order terms, and if the crack propagates along a curved path, as being shown in Liu and Rosakis (1992), it also relates to the shape of the crack trajectory. At this point, we have clearly known the asymptotic structure of the deformation field near a transiently moving crack-tip. Because each term in the expansion is associated with certain function of the radial distance from the crack-tip, therefore, in order to correctly interpret the observation data in an experimental investigation, either we can change the observation position continuously so that we can pick up one specific information we are interested in, or we cannot choose the observation point freely so that we have to resolve various information from the data we get. The dependence of the leading term on the radial distance is $r^{-1/2}$, so the effects of this term are restrained inside the region very close to the moving crack-tip. However, the dependence of the higher order terms on the radial distance is $r^{1/2}$ or higher. As a result, as the observation position is relatively far away from the crack-tip, the effects of the higher order terms will become profound and cannot be

neglected in any attempt to interpret data obtained at that position.

The experimental configuration developed by Ravichandran and Clifton (1989) and by Prakash and Clifton (1992) has the great advantage of being correlated to the existing analytical results for two-dimensional dynamic fracture problems. However, the technique utilized by Ravichandran and Clifton (1989) and by Prakash and Clifton (1992) cannot access the crack-tip, so that the direct information about the crack-tip speed and the intensity or the amplitude of the local stress and deformation fields can only be inferred from the information obtained at positions far away from the moving crack-tip. Nevertheless, this experimental configuration is still a very good candidate for the study of dynamic fracture behavior of materials under very high loading rates while the transient effects associated with the crack growth should be taken into account in the interpretation.

In the first part of this chapter, the mathematical problem by which the experimental and loading configuration can be modeled, is revisited, and the full field solution for the stresses is obtained. Meanwhile, the coefficients that appear in the transient asymptotic representation of the deformation field are also be obtained for the situation of crack propagating with constant speed. By including the higher order terms in the theoretical simulation, the result agrees fairly well with the experimental observations (see Fig.12). We can conclude from Fig.12 that the near tip deformation field is well described by the higher order transient asymptotic expansion, at least qualitatively. Since the experimental technique cannot provide the complete histories of the crack motion, we have to suppose that the crack growth is governed by a criterion which relates the critical dynamic stress intensity factor and the moving speed of the crack-tip. The mathematical form of this criterion is motivated by previous experimental measurements. Through solving the crack-tip equation of motion, the history of crack-tip motion can be determined, so are those quantities related to the transient effects. When all of these transient effects related quantities are cooperated into the asymptotic representation of the particle velocity near the crack-tip, the simulation has become very close to the experimental observation. The meaning of this simulation has two folds. One shows again the necessity of applying the higher order asymptotic expansion which includes the transient history of the crack growth to describe the near tip deformation fields. The other one shows that the crack growth is indeed controlled by a material related criterion. This criterion gives the unique relationship between the dynamic fracture toughness K_{IC}^{d} and the crack-tip speed v. The existence of such a crite-

rion in this simulation is supported by using the higher order transient expansion, while the lack of the uniqueness of a relationship between K_{IC}^d and v has been observed when the K_I^d-dominant assumption or the steady state higher order expansion is used (see Kobayashi and Mall, 1978, and Ravi-Chandar and Knauss, 1984). Therefore, the lack of the uniqueness of correspondence between K_{IC}^d and v may be attributed by the fact that there is no K_I^d-dominant deformation field surrounding the crack-tip close to the crack initiation as has been prevailed in Section 2 and the study by Ma and Freund (1986).

However, some difficulties still exist preventing the complete simulation of the experimental observations by using the existing analytical solutions. This is due to the presence of free boundary in the experimental configuration. Complicated wave reflections will occur when the stress waves emanated from the stationary or the moving crack-tip reach the boundary. These reflections impose new difficulty for obtaining complete analytical solution. As a result, in order to deepen the understanding of the mechanism of dynamic crack initiation and growth, detailed numerical simulation should be performed.

Acknowledgements

The authors would like to acknowledge extensive discussions with Professor L. B. Freund of Brown University. The generous support of the Office of Naval Research through Grant N00014-90-J-1340 and of the Army Research Office through Grant DAAH04-93-G-0037 is also acknowledged.

References

Achenbach, J.D., (1973), *Wave Propagation in Elastic Solids*, North-Holland.

Achenbach, J.D. and Nuismer, R., (1971), "Fracture generated by a dilatational wave," *International Journal of Fracture* **7**, pp.77–88.

Baker, B. R., (1962), "Dynamic stresses created by a moving crack," *Journal of Applied Mechanics*, **29**(3), pp.449–458.

Beinert, J. and Kalthoff, J. F., (1983), "The development of a crack arrest test specimen with reduced dynamic effects," in *Application of Fracture*

Mechanics to Materials and Structures, edited by Sih, G. C., *et al.*, pp.493–511.

Freund, L. B., (1973), "Crack propagation in an elastic solid subjected to general loading. III. Stress wave loading," *Journal of the Mechanics and Physics of Solids* **21**, pp.47–61.

Freund, L. B., (1990), *Dynamic Fracture Mechanics*, Cambridge University Press.

Freund, L. B. and Clifton, R. J., (1974), "On the uniqueness of plane elastodynamic solutions for running cracks," *Journal of Elasticity*, **4**(4), pp.293–299.

Freund, L. B. and Rosakis, A. J., (1992), "The structure of the near-tip field during transient elastodynamic crack growth," *Journal of the Mechanics and Physics of Solids*, **40**(3), pp.699–719.

Kalthoff, J. F., Beinert, J., and Winkler, S., (1979), "Analysis of fast running arresting cracks by the shadow-optical method of caustics," *Proceedings of the IUTAM symposium on Optical Methods in Mechanics of Solids*, edited by Lagarde, A., Poitiers, France, pp.497–508.

Kobayashi, T. and Dally, J. W., (1980), "Dynamic photo-elastic determination of the $\dot{a} - K$ relation for the 4340 steel," in *Crack Arrest Methodology and Applications*, edited by Hahn, G. T., *et al.*, *ASTM STP 711*, pp.189–210.

Kobayashi, A. S. and Mall, S., (1978), "Dynamic fracture toughness of Homalite 100," *Experimental Mechanics*, **18**, pp.11–18.

Krishnaswamy, S. and Rosakis, A. J., (1991), "On the extent of dominance of asymptotic elastodynamic crack-tip fields: Part I – An experimental study using bifocal caustics," *Journal of Applied Mechanics*, **58**(1), pp.87–94.

Krishnaswamy, S., Tippur, H. V., and Rosakis, A. J., (1992), "Measurement of transient crack tip deformation fields using the method of coherent gradient sensing," *Journal of the Mechanics and Physics of Solids*, **40**(2), pp.339–372.

Liu, C. and Rosakis, A. J., (1992), "On the higher order asymptotic analysis of a non-uniformly propagating dynamic crack along an arbitrary path," SM Report 92–45, Graduate Aeronautical Laboratories, California Institute of Technology. To appear in the *Journal of Elasticity* (1994).

Liu, C., Rosakis, A. J., and Freund, L. B., (1993)], "The interpretation of optical caustics in the presence of dynamic non-uniform crack-tip motion histories: A study based on a higher order transient crack-tip expansion," *International Journal of Solids and Structures*, **30**(7), pp.875–897.

Ma, C. C. and Freund, L. B., (1986), "The extent of the stress intensity factor field during crack growth under dynamic loading conditions," *Journal of Applied Mechanics* **53**, pp.303–310.

Prakash, V. and Clifton, R. J., (1992), "Experimental and analytical investigation of dynamic fracture under conditions of plane strain," *Fracture Mechanics: Twenty-Second Symposium (Volume I), ASTM STP 1131*, edited by Ernst, H. A. *et al.*, American Society for Testing and Materials, Philadelphia, 1992, pp.412–444.

Prakash, V., Freund, L. B., and Clifton, R. J., (1992), "Stress wave radiation from a crack tip during dynamic initiation," *Journal of Applied Mechanics*, **59**(2), pp.356–365.

Ravi-Chandar, K. and Knauss, W. G., (1982), "Dynamic crack-tip stresses under stress wave loading – A comparison of theory and experiment," *International Journal of Fracture* **20**, pp.209–222.

Ravi-Chandar, K. and Knauss, W. G., (1984), "An experimental investigation into the mechanics of dynamic fracture: I. Crack initiation and arrest," *International Journal of Fracture*, **25**, pp.247–262.

Ravichandran, G. and Clifton, R. J., (1989), "Dynamic fracture under plane wave loading," *International Journal of Fracture*, **40**, pp.157–201.

Rosakis, A. J., (1993), "Two optical techniques sensitive to gradients of optical path difference: The method of caustics and the coherent gradient sensor (CGS)," in *Experimental Techniques in Fracture*, **3**, edited by J. Epstein, Chapter 10, pp.327–425.

Rosakis, A. J., Duffy, J., and Freund, L. B., (1984), "The determination of dynamic fracture toughness of AISI 4340 steel by the shadow spot method," *Journal of the Mechanics and Physics of Solids*, **32**, pp.443–460.

Rosakis, A. J., Liu, C., and Freund, L. B., (1991), "A note on the asymptotic stress field of a non-uniformly propagating dynamic crack," *International Journal of Fracture*, **50**, R39–R45.

Rosakis, A. J. and Ravi-Chandar, K., (1986), "On crack-tip stress state: An experimental evaluation of three-dimensional effects," *International Journal of Solids and Structures*, **22**(2), pp.121–134.

van der Pol, B. and Bremmer, H., (1955), *Operational Calculus*, Second edition. Cambridge University Press.

Willis, J. R., (1992), "The stress field near the tip of an accelerating crack," *Journal of the Mechanics and Physics of Solids*, **40**(7), pp.1671–1681.

Yang, W. and Freund, L. B., (1985), "Transverse shear effects for through cracks in an elastic plate," *International Journal of Solids and Structures*, **21**(9), pp.977–994.

Yoffe, E. H., (1951), "The moving griffith crack," *Philosophical Magazine*, **42**, pp.739–750.

Zehnder, A. T. and Rosakis, A. J., (1990), "Dynamic fracture initiation and propagation in 4340 steel under impact loading," *International Journal of Fracture*, **43**(4), pp.271–285.

Appendix: Inversion of Laplace transforms – Cagniard-de Hoop technique

Consider a quantity $G(\zeta, x_2, s)$ with the form

$$G(\zeta, x_2, s) = \frac{A(\zeta)}{s^2} e^{-s\alpha^{(B)}(\zeta)x_2}, \tag{1}$$

where $A(\zeta)$ is analytic in the strip $-a < \mathrm{Re}\,\zeta < a$. The inversion of $G(\zeta, x_2, s)$ is given by

$$\hat{g}(x_1, x_2, s) = \frac{1}{2\pi si} \int_{\zeta_0 - i\infty}^{\zeta_0 + i\infty} A(\zeta) e^{-\{\alpha^{(B)}(\zeta)x_2 - \zeta x_1\}s} \mathrm{d}\zeta, \tag{2}$$

where ζ_0 is real and $-a < \zeta_0 < a$. Set

$$\alpha^{(B)}(\zeta)x_2 - \zeta x_1 = \tau > 0, \tag{3}$$

and solve eqn (3) for ζ, we obtain

$$\zeta_{l\pm}^{(B)} = -\frac{\tau}{r}\cos\theta \pm i\sqrt{\frac{\tau^2}{r^2} - a^2}\sin\theta, \tag{4}$$

where

$$r = \sqrt{x_1^2 + x_2^2}, \qquad \theta = \tan^{-1}\frac{x_2}{x_1}.$$

Notice that

$$\left.\begin{aligned} &\operatorname{Im}\zeta_{l\pm}^{(\mathrm{B})} = 0, && \text{as } \tau = a\tau \\ &\frac{\operatorname{Im}\zeta_{l\pm}^{(\mathrm{B})}}{\operatorname{Re}\zeta_{l\pm}^{(\mathrm{B})}} = \mp\tan\theta, && \text{as } \tau \to \infty \end{aligned}\right\}. \tag{5}$$

From Fig.1 and the analysis above, we can see that the original integral contour Γ_i can be distorted into new integral contours $\zeta_{l+}^{(\mathrm{B})}$ and $\zeta_{l-}^{(\mathrm{B})}$, and the new contour will not intersect with the branch cuts as θ changing from 0 to π.

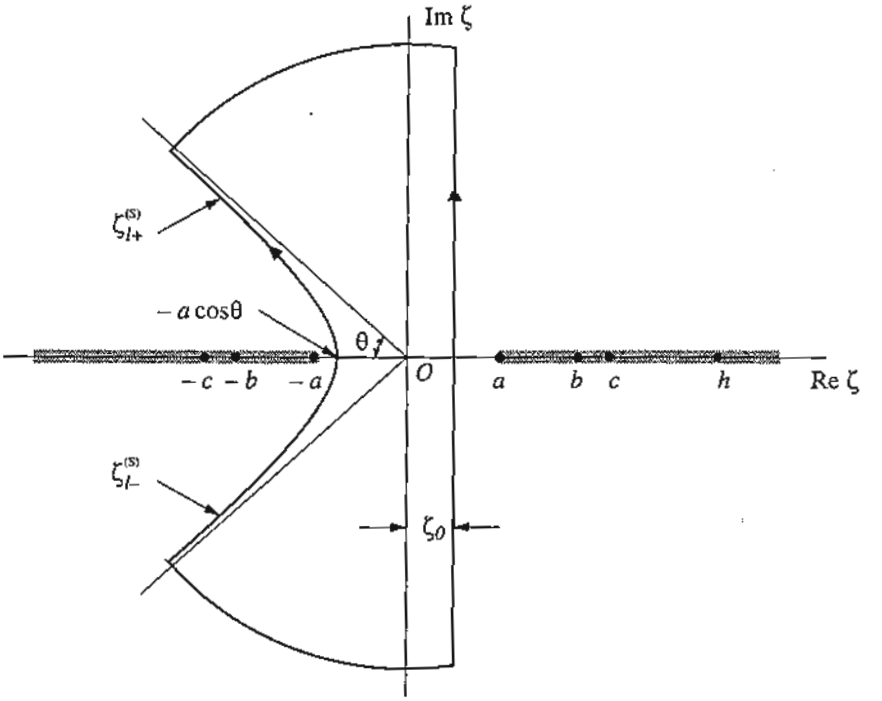

Figure 1: Distortion of the integral contour to evaluate the inversion of $G(\zeta, x_2, s)$.

Now, we can express $\hat{g}(x_1, x_2, s)$ as

$$\hat{g}(x_1, x_2, s) = \frac{1}{2\pi s i}\int_{ar}^{\infty}\left\{A(\zeta_{l+}^{(\mathrm{B})})\frac{\partial\zeta_{l+}^{(\mathrm{B})}}{\partial\tau} - A(\zeta_{l-}^{(\mathrm{B})})\frac{\partial\zeta_{l-}^{(\mathrm{B})}}{\partial\tau}\right\}e^{-s\tau}\mathrm{d}\tau. \tag{6}$$

Notice that $\zeta_{l-}^{(\mathrm{B})} = \overline{\zeta}_{l+}^{(\mathrm{B})}$. If $A(\zeta)$ has the property $\overline{A(\zeta)} = A(\overline{\zeta})$, then

$$\hat{g}(x_1, x_2, s) = \frac{1}{\pi s}\int_{ar}^{\infty}\operatorname{Im}\left\{A(\zeta_{l+}^{(\mathrm{B})})\frac{\partial\zeta_{l+}^{(\mathrm{B})}}{\partial\tau}\right\}e^{-s\tau}\mathrm{d}\tau. \tag{7}$$

Furthermore,

$$g(x_1, x_2, t) = \frac{1}{2\pi i} \int_{\sigma - i\infty}^{\sigma + i\infty} \hat{g}(x_1, x_2, s) e^{st} \mathrm{d}s. \tag{8}$$

After some manipulations, it can be shown that

$$g(x_1, x_2, t) = \frac{1}{\pi} \int_{ar}^{t} \mathrm{Im} \left\{ A(\zeta_{l+}^{(\mathrm{B})}) \frac{\partial \zeta_{l+}^{(\mathrm{B})}}{\partial \tau} \right\} \mathrm{d}\tau \cdot H(t - a\tau), \tag{9}$$

where $\zeta_{l+}^{(\mathrm{B})}(x_1, x_2, t)$ is given by eqn (4), from which $\partial \zeta_{l+}^{(\mathrm{B})} / \partial \tau$ can also be calculated.

On the other hand, if $G(\zeta, x_2, s)$ has the form

$$G(\zeta, x_2, s) = \frac{A(\zeta)}{s^2 \zeta} e^{-s\alpha^{(\mathrm{B})}(\zeta) x_2}, \tag{10}$$

where $A(\zeta)$ is analytic in the strip $-a < \mathrm{Re}\ \zeta < a$. Write

$$A(\zeta, x_2, s) = \frac{A(\zeta)}{s} e^{-s\alpha^{(\mathrm{B})}(\zeta) x_2},$$

then the inversion of $A(\zeta, x_2, s)$ can be obtained by using the Cagniard-de Hoop technique we just discussed. It is

$$\hat{a}(x_1, x_2, s) = \frac{1}{\pi} \int_{ar}^{\infty} \mathrm{Im} \left\{ A(\zeta_{l+}^{(\mathrm{B})}) \frac{\partial \zeta_{l+}^{(\mathrm{B})}}{\partial \tau} \right\} e^{-s\tau} \mathrm{d}\tau. \tag{11}$$

Notice that for the Heaviside function $H(x_1)$, we have

$$\int_{-\infty}^{\infty} H(x_1) e^{-s\zeta x_1} \mathrm{d}x_1 = 1, \quad \text{for } \mathrm{Re}\ \zeta > 0.$$

From the composition product relation (van der Pol and Bremmer, 1955), the inversion of $G(\zeta, x_2, s)$ which can be rewritten as

$$G(\zeta, x_2, s) = \frac{A(\zeta, x_2, s)}{s\zeta} \cdot 1,$$

is given by

$$\hat{g}(x_1, x_2, s) = \int_{-\infty}^{\infty} \hat{a}(x_1^*, x_2, s) H(x_1 - x_1^*) \mathrm{d}x_1^*, \tag{12}$$

or

$$\hat{g}(x_1, x_2, s) = \frac{1}{\pi} \int_{-\infty}^{x_1} \left\{ \int_{ar^*}^{\infty} \mathrm{Im} \left[A(\zeta_{l+}^{(\mathrm{B})*}) \frac{\partial \zeta_{l+}^{(\mathrm{B})*}}{\partial \tau} \right] e^{-s\tau} \mathrm{d}\tau \right\} \mathrm{d}x_1^*, \tag{13}$$

where

$$\zeta_{l+}^{(\mathrm{B})*} = -\frac{\tau}{\tau^*} \cos\theta^* + i \sqrt{\frac{\tau^2}{\tau^{*2}} - a^2} \sin\theta^*,$$

and

$$r^* = \sqrt{x_1^{*2} + x_2^2}, \qquad \theta^* = \tan^{-1}\frac{x_2}{x_1^*}.$$

Also, by performing the inversion of the Laplace transform with respect to parameter s, we can get

$$g(x_1, x_2, t) = \frac{1}{\pi}\int_{-\infty}^{x_1} \mathrm{Im}\left\{A(\zeta_{l+}^{(\mathrm{B})*})\frac{\partial \zeta_{l+}^{(\mathrm{B})*}}{\partial t}\right\} H(t - ar^*)\mathrm{d}x_1^*, \tag{14}$$

or

$$g(x_1, x_2, t) = \frac{1}{\pi}\int_{-\omega_l}^{\mathrm{Min}(x_1, \omega_l)} \mathrm{Im}\left\{A(\zeta_{l+}^{(\mathrm{B})*})\frac{\partial \zeta_{l+}^{(\mathrm{B})*}}{\partial t}\right\} \mathrm{d}x_1^*, \tag{15}$$

where

$$\omega_l = \left(\frac{t^2}{a^2} - x_2^2\right)^{1/2}.$$

Finally, we have

$$g(x_1, x_2, t) = \frac{1}{\pi}\int_{-\omega_l}^{x_1} \mathrm{Im}\left\{A(\zeta_{l+}^{(\mathrm{B})*})\frac{\partial \zeta_{l+}^{(\mathrm{B})*}}{\partial t}\right\} \mathrm{d}x_1^* \cdot H(t - ar). \tag{16}$$

Consider another quantity $W(\zeta, x_2, s)$ with the form

$$W(\zeta, x_2, s) = \frac{B(\zeta)}{s^2} e^{-s\beta^{(\mathrm{B})}(\zeta)x_2}, \tag{17}$$

where $B(\zeta)$ is analytic in the strip $-b < \mathrm{Re}\ \zeta < a$. By definition,

$$\hat{w}(x_1, x_2, s) = \frac{1}{2\pi s i}\int_{\zeta_0 - i\infty}^{\zeta_0 + i\infty} B(\zeta) e^{-\{\beta^{(\mathrm{B})}(\zeta)x_2 - \zeta x_1\}s}\mathrm{d}\zeta, \tag{18}$$

where ζ_0 is real and $-b < \zeta_0 < a$. Similar to previous discussions, we may set

$$\beta^{(\mathrm{B})}(\zeta)x_2 - \zeta x_1 = \tau > 0, \tag{19}$$

and solve eqn (19) for ζ. Then

$$\zeta_{s\pm}^{(\mathrm{B})} = -\frac{\tau}{r}\cos\theta \pm i\sqrt{\frac{\tau^2}{r^2} - b^2}\sin\theta. \tag{20}$$

We also have the property that

$$\left.\begin{array}{ll} \mathrm{Im}\ \zeta_{s\pm}^{(\mathrm{B})} = 0, & \text{as } \tau = br \\ \dfrac{\mathrm{Im}\ \zeta_{s\pm}^{(\mathrm{B})}}{\mathrm{Re}\ \zeta_{s\pm}^{(\mathrm{B})}} = \mp\tan\theta, & \text{as } \tau \to \infty \end{array}\right\}. \tag{21}$$

But it can be seen that as $\tau = b\tau$,

$$\zeta_{s\pm}^{(\mathrm{B})} = -b\cos\theta = \lambda^{(\mathrm{B})}(\theta),$$

and as a result, when θ is changing from 0 to π, $\lambda^{(\mathrm{B})}(\theta)$ is in the range

$$-b \le \lambda^{(\mathrm{B})}(\theta) \le b.$$

So, as θ is greater than angle $\theta_{\mathrm{H}}^{(\mathrm{B})} = \pi - \cos^{-1}(a/b)$, the distorted integral contour will intersect with the branch cut, and we need to consider two cases separately.

For $0 \le \theta \le \theta_{\mathrm{H}}^{(\mathrm{B})}$, we can directly apply the same procedure for $G(\zeta, x_2, s)$, and if $B(\zeta)$ satisfies that $\overline{B(\zeta)} = B(\bar{\zeta})$, then

$$w(x_1, x_2, t) = \frac{1}{\pi}\int_{br}^{t} \mathrm{Im}\left\{ B(\zeta_{s+}^{(\mathrm{B})}) \frac{\partial \zeta_{s+}^{(\mathrm{B})}}{\partial \tau} \right\} \mathrm{d}\tau \cdot H(t - b\tau), \tag{22}$$

where $\zeta_{s+}^{(\mathrm{B})}(x_1, x_2, t)$ is given by eqn (20), from which $\partial\zeta_{s+}^{(\mathrm{B})}/\partial\tau$ can be calculated.

For $\theta_{\mathrm{H}}^{(\mathrm{B})} \le \theta \le \pi$, from Fig.2, we have

$$\hat{w}(x_1, x_2, s) = \hat{w}_0(x_1, x_2, s) + \hat{w}_H(x_1, x_2, s), \tag{23}$$

where by assuming that $\overline{B(\zeta)} = B(\bar{\zeta})$,

$$\hat{w}_0(x_1, x_2, s) = \frac{1}{\pi s}\int_{br}^{\infty} \mathrm{Im}\left\{ B(\zeta_{s+}^{(\mathrm{B})}) \frac{\partial \zeta_{s+}^{(\mathrm{B})}}{\partial \tau} \right\} e^{-s\tau}\mathrm{d}\tau,$$

and

$$\hat{w}_H(x_1, x_2, s) = \frac{1}{\pi s}\int_{a}^{\lambda^{(\mathrm{B})}(\theta)} \mathrm{Im}\left\{ B^{+}(\eta) \right\} e^{-\{\beta^{(\mathrm{B})}(\eta)x_2 - \eta x_1\}s}\mathrm{d}\eta.$$

Moreover, it can be shown that

$$w_0(x_1, x_2, t) = \frac{1}{\pi}\int_{br}^{t} \mathrm{Im}\left\{ B(\zeta_{s+}^{(\mathrm{B})}) \frac{\partial \zeta_{s+}^{(\mathrm{B})}}{\partial \tau} \right\} \mathrm{d}\tau \cdot H(t - b\tau), \tag{24}$$

and

$$w_H(x_1, x_2, t) = \frac{1}{\pi}\int_{a}^{\lambda^{(\mathrm{B})}(\theta)} \mathrm{Im}\left\{ B^{+}(\eta) \right\} h^{(\mathrm{B})}(\eta)\mathrm{d}\eta, \tag{25}$$

where

$$h^{(\mathrm{B})}(\eta) = H\left(t - [\beta^{(\mathrm{B})}(\eta)x_2 - \eta x_1]\right), \quad a < \eta \le \lambda^{(\mathrm{B})}(\theta).$$

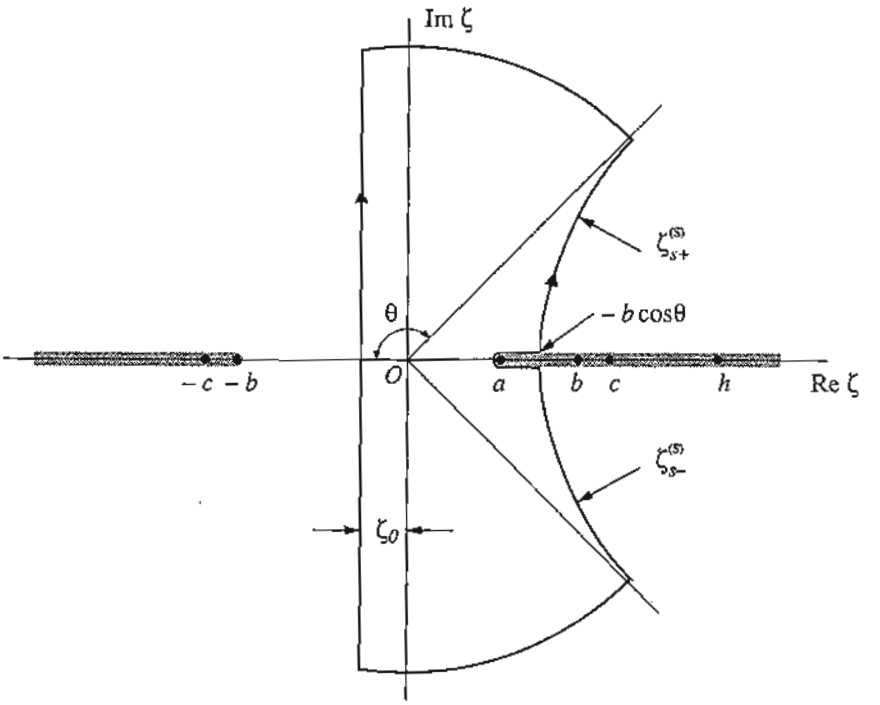

Figure 2: Distortion of the integral contour to evaluate the inversion of $W(\zeta, x_2, s)$.

Summarize the results for above two cases, we can write

$$w(x_1,x_2,t) = \frac{1}{\pi}\left\{\begin{array}{l}\displaystyle\int_{b\tau}^{t} \mathrm{Im}\left[B(\zeta_{s+}^{(\mathrm{B})})\frac{\partial\zeta_{s+}^{(\mathrm{B})}}{\partial\tau}\right]\mathrm{d}\tau\cdot H(t-b\tau) \\ \displaystyle+\int_{a}^{\lambda^{(\mathrm{B})}(\theta)} \mathrm{Im}\left[B^{+}(\eta)\right]h^{(\mathrm{B})}(\eta)\mathrm{d}\eta\cdot H(\theta-\theta_{\mathrm{H}}^{(\mathrm{B})})\end{array}\right\}. \quad (26)$$

As a matter of fact, the second part in the right-hand side of eqn (26) provides the information inside the region of head wave. By denoting $\zeta_{l,s+}^{(\mathrm{B})}$ as $\zeta_{l,s}^{(\mathrm{B})}$, expressions in (13) and (15) are obtained. By using the same technique, expressions in (24) and (25) can also be obtained.